University of Alberta

Dropwise Condensation (DWC) Heat Transfer on Self-Assembled Monolayers (SAMs)

by

Guoxin Pang

©

A thesis submitted to the Faculty of Graduate Studies and Research in partial fulfillment of the requirements for the degree of Master of Science.

Department of Mechanical Engineering

Edmonton, Alberta
Fall 2004

Library and Archives Canada

Published Heritage Branch

395 Wellington Street
Ottawa ON K1A 0N4
Canada

Bibliothèque et Archives Canada

Direction du Patrimoine de l'édition

395, rue Wellington
Ottawa ON K1A 0N4
Canada

Your file Votre référence
ISBN: 0-612-95830-2
Our file Notre référence
ISBN: 0-612-95830-2

The author has granted a non-exclusive license allowing the Library and Archives Canada to reproduce, loan, distribute or sell copies of this thesis in microform, paper or electronic formats.

The author retains ownership of the copyright in this thesis. Neither the thesis nor substantial extracts from it may be printed or otherwise reproduced without the author's permission.

L'auteur a accordé une licence non exclusive permettant à la Bibliothèque et Archives Canada de reproduire, prêter, distribuer ou vendre des copies de cette thèse sous la forme de microfiche/film, de reproduction sur papier ou sur format électronique.

L'auteur conserve la propriété du droit d'auteur qui protège cette thèse. Ni la thèse ni des extraits substantiels de celle-ci ne doivent être imprimés ou aturement reproduits sans son autorisation.

In compliance with the Canadian Privacy Act some supporting forms may have been removed from this thesis.

While these forms may be included in the document page count, their removal does not represent any loss of content from the thesis.

Conformément à la loi canadienne sur la protection de la vie privée, quelques formulaires secondaires ont été enlevés de cette thèse.

Bien que ces formulaires aient inclus dans la pagination, il n'y aura aucun contenu manquant.

Canada

"Imagination is more important than knowledge."

–Albert Einstein

To my wife, Wei for the other memorable moment during this pursuit:

the birth of our son, Ge'er.

ACKNOWLEDGEMENTS

My acknowledgment list is pretty well endless, but I will try to fit everybody in. I would like to start by thanking my family: my wife Wei, my son Ge'er, my parents and my in-laws for the support the whole way during this pursuit.

The second most important people I would like to thank are all the teachers that have helped me along the way. Here at the University of Alberta, almost every professor has given me inspiration of one form or another. On top of the list is my supervisor Dr. D. Y. Kwok. And also, I would like to mention the others' names here: Dr. J. D. Dale,Dr. Q. Liu, Dr. Z. Xia and Dr. S. Liu.

Special thanks to all the machinists and technicians: Andrew Coward, Dirk Kelm, Albert Yeun, Dave Pape, Terri Nord, Rick Bubenko, Bernie Faulkner and Ian Buttar whose knowledge and abilities helped me a great deal.

Finally, I would like to say thank you to all colleagues in our group for the very helpful discussion, especially to Kelvin Isaacson and Yu-Wen Chang who make it easy to study in this lab.

I am greatly appreciative of the guidance that you have given me.

Contents

1 Introduction 1

2 Literature Review 3

2.1 Dropwise Condensation (DWC) Heat Transfer 3

2.1.1 Organic Materials 3

2.1.2 Noble Metal Coatings 3

2.1.3 Thin-layer Organic Coatings 4

2.2 Self-Assembled Monolayers (SAMs) 7

2.2.1 Self-Assembly Systems 7

2.2.2 Self-Assembled Monolayers (SAMs) on Gold 8

2.2.3 Self-Assembled Monolayers (SAMs) on Copper 11

2.2.4 Thermal Stability of SAMs 12

2.3 Summary 14

3 Experimental Procedures 16

3.1 Contact Angle Hysteresis 16

3.2 Sample Preparation 19

3.2.1 Condenser Surface Polishing 19
3.2.2 Thermal Evaporation 21
3.2.3 Deposition of SAMs 22
3.3 Experimental apparatus 23
3.3.1 Fourier Transform Infrared Spectroscopy (FT-IR) 23
3.3.2 Spectroscopic Ellipsometry 24
3.3.3 Experimental Set-up 25
3.4 Measurement Principle 28

4 Results and Discussion **39**
4.1 Application of SAMs at Same Heat Flux 39
4.1.1 Improvement of Heat Transfer Coefficient 39
4.1.2 Characterizations of SAMs 42
4.2 Application of SAMs at Different Heat fluxes 48
4.2.1 Film Condensation 48
4.2.2 Dropwise Condensation 51

5 Conclusions and Future Research **67**
5.1 Conclusions 67
5.2 Future Work 68

References **70**

List of Tables

3.1 Calibration values of the four thermocouple probes. 31

3.2 Calibration values of the three thermocouple wires. 32

3.3 Factors that affect the maximum error of temperature measurements. 33

3.4 Factors that affect the maximum error of distance measurements. . 34

List of Figures

2.1 Schematic of a highly ordered monolayer of alkanethiolate formed on a gold surface. 9

3.1 Schematic of the rectangular copper block. 17

3.2 Profile of a drop on an inclined surface. 18

3.3 Schematic of the deposition of alkanethiol SAMs on a copper surface. 22

3.4 Schematic of an experimental set-up for the measurements of the condensation heat transfer coefficient. 25

3.5 An exploded view of the condensation test assembly. 26

3.6 Schematic of the measurement system of the copper block condenser. 29

3.7 Polynomial regression curve-fitting of copper thermal conductivity. . 30

3.8 Polynomial regression curve-fitting of air thermal conductivity. . . . 35

3.9 Temperature profile of the copper block under one-dimensional steady-state conduction heat transfer process obtained by a finite element analysis through ANSYS 7.0. 36

3.10 Polynomial regression curve-fittings of the four thermocouple probes. 37

3.11 Polynomial regression curve-fittings of the three thermocouple wires. 38

4.1 Condensation heat transfer coefficient of SAMs on evaporated Au/Ti/Cu substrates as a function of time during steam condensation at standard atmosphere pressure. Steam velocity passing through the condensing surface is ~ 6 m/s and heat flux is ~ 280 kW/m^2. 40

4.2 Dropwise condensation of steam on self-assembled monolayers (SAMs) derived from 1-octadecanethiol [$HS(CH_2)_{17}CH_3$] onto gold-coated-copper substrates. 41

4.3 Reflectance FT-IR spectra for SAMs derived from 1-octadecanethiol on Au/Ti/Cu substrates subjected to steam condensation in various duration ($q'' \approx 280$ kW/m^2). The dashed lines represent the positions of the original modes for a trans-extended monolayer. The spectra have been offset for clarity. 43

4.4 Normalized thickness of SAMs derived from 1-octadecanethiol on gold-coated-copper substrates as a function of condensation duration for heat flux $q'' \approx 280$ kW/m^2. t_0 is the initial film thickness reference. Error bars are $\pm$ 0.2 nm in reference to t_0 and represent typical measurement errors for ellipsometry. 44

4.5 Normalized heat transfer coefficient as a function of condensation duration for heat flux $q'' \approx 280$ kW/m^2. h_0 is the heat transfer coefficient after 10 minute condensation. Error bars are 95% confidence limits. 45

4.6 Experimental and theoretical film condensation heat transfer coefficients of 16-mercaptohexadecanoic acid SAMs on evaporated Au/Ti/Cu substrates as a function of time during steam condensation: (a) $q'' \approx$ 140 kW/m^2; (b) $q'' \approx$ 200 kW/m^2; (c) $q'' \approx$ 230 kW/m^2; (d) $q'' \approx$ 270 kW/m^2. 50

4.7 Heat transfer coefficient as a function of condensation duration for heat flux $q'' \approx$ 320 kW/m^2. Error bars are 95% confidence limits. . 53

4.8 Heat transfer coefficient as a function of condensation duration for heat flux $q'' \approx$ 360 kW/m^2. Error bars are 95% confidence limits. . 54

4.9 Heat transfer coefficient as a function of condensation duration for heat flux $q'' \approx$ 400 kW/m^2. Error bars are 95% confidence limits. . 55

4.10 Heat transfer coefficient as a function of condensation duration for heat flux $q'' \approx$ 460 kW/m^2. Error bars are 95% confidence limits. . 56

4.11 Reflectance FT-IR spectra for SAMs derived from 1-octadecanethiol on Au/Ti/Cu substrates subjected to steam condensation in various duration ($q'' \approx$ 320 kW/m^2). The dashed lines represent the positions of the original modes for a trans-extended monolayer. The spectra have been offset for clarity. 61

4.12 Reflectance FT-IR spectra for SAMs derived from 1-octadecanethiol on Au/Ti/Cu substrates subjected to steam condensation in various duration ($q'' \approx$ 360 kW/m^2). The dashed lines represent the positions of the original modes for a trans-extended monolayer. The spectra have been offset for clarity. 62

4.13 Reflectance FT-IR spectra for SAMs derived from 1-octadecanethiol on Au/Ti/Cu substrates subjected to steam condensation in various duration ($q'' \approx 400$ kW/m^2). The dashed lines represent the positions of the original modes for a trans-extended monolayer. The spectra have been offset for clarity. 63

4.14 Reflectance FT-IR spectra for SAMs derived from 1-octadecanethiol on Au/Ti/Cu substrates subjected to steam condensation in various duration ($q'' \approx 460$ kW/m^2). The dashed lines represent the positions of the original modes for a trans-extended monolayer. The spectra have been offset for clarity. 64

4.15 Normalized thickness of SAMs derived from 1-octadecanethiol on Au/Ti/Cu substrates as a function of condensation duration for different heat fluxes. t_0 is the initial film thickness reference. 65

4.16 Normalized heat transfer coefficient of SAMs derived from 1-octadecanethiol on Au/Ti/Cu substrates as a function of condensation duration for different heat fluxes. h_0 is the heat transfer coefficient after 10 minute condensation. 66

NOMENCLATURE

ENGLISH SYMBOLS

A	Cross-section area of the condensing chamber, m^2
g	Gravitational acceleration, m/s^2
h	Condensation heat transfer coefficient, $kW/m^2 \cdot K$
h_0	Initial (10 minutes later) condensation heat transfer coefficient, $kW/m^2 \cdot K$
K	Thermal conductivity of copper, $W/m \cdot K$
k	Reflective index of the material
m	Mass of the droplet, kg
m'	Critical mass of the droplet, kg
$\dot{m}$	Mass flow rate, g/s

n	Refractive index of the material
P	Pressure, kPa
q''	Heat flux, kW/m^2
T	Temperature, K
t	Thickness of self-assembled monolayers, nm
t_0	Initial thickness of self-assembled monolayers, nm
t'	Time, minute
X	Heat transfer direction along the copper block height

GREEK SYMBOLS

α	Angle of the inclined surface, °
γ_{lv}	Surface tension of the liquid-vapor interface, mJ/m^2
δ	Distance, mm
θ_a	Advancing contact angle, °
θ'_a	Critical advancing contact angle, °

θ_r	Receding contact angle, °
θ_r'	Critical receding contact angle, °
λ	Wavelength, nm
ν_a	Peak position of the asymmetric C-H stretching mode in reflection-infrared spectra
ν_s	Peak position of the symmetric C-H stretching mode in reflection-infrared spectra
ρ	Steam density, kg/m^3
υ	Steam velocity, m/s

Chapter 1

Introduction

Condensation occurs when the temperature of a vapor is reduced below its saturation temperature. In an industrial application, the process commonly results from contact between a vapor and a cool surface. Depending on the wettability of a surface, condensation may result in one of two ways. For steam condensation, if the surface is hydrophilic, that means it is a high energy surface, the condensate forms a continuous film on the cool surface. The heat transfer coefficients of the order of $5 \sim 10$ kW/m^2·K are expected for film condensation. However, if the surface is coated with a substance which is strongly adhered to the condensing surface and repels the water (this substance is called a promoter), the surface becomes low energy and hydrophobic, dropwise condensation (DWC) will be the dominant form. The heat transfer coefficients are more than an order of magnitude larger than those associated with film condensation.

Due to the much higher heat transfer coefficient of DWC, considerable attention have been given towards the development of suitable DWC promoters. Recently, self-assembled monolayers (SAMs) were applied to investigate the DWC

heat transfer of steam because of its strong potential as long-term DWC promoters. However, it is noted that, although surface properties are crucial factors in DWC, there has been very little effort in the literature to relate the enhanced heat transfer coefficient directly with surface properties, chemistries, and property changes over time; documentation of the procedures for surface preparation and characterization are surprisingly limited.

In this study, an integrated study of dropwise condensation heat transfer of steam on self-assembled monolayers of 1-octadecanethiol [$CH_3(CH_2)_{17}SH$] and 16-mercaptohexadecanoic acid [$CO_2H(CH_2)_{15}SH$] adsorbed onto gold-coated-copper substrates is presented. The choice of these SAMs allows a systematic surface energetic variation in relation to the enhanced heat transfer coefficient. A durability test was conducted by relating the heat transfer coefficient to changes in monolayer thickness and chemistry with time and heat flux through a spectroscopic ellipsometry and a fourier transform infrared spectroscopy (FT-IR), respectively. The results indicate clearly the presence of a time and heat flux dependent dynamic process for the organic surfaces during DWC process.

Chapter 2

Literature Review

2.1 Dropwise Condensation (DWC) Heat Transfer

Since it was first reported in 1930 by Schmidt *et al.* [1], DWC has been of interest to many investigators. The key point to this question has been, and is, to develop reliable and long-lived DWC promoters.

2.1.1 Organic Materials

Organic materials (such as waxes, oils, and greases) were applied to achieve DWC of steam in early 1960s, but these promoters were washed off rapidly and the condensation reverted to filmwise quickly.

2.1.2 Noble Metal Coatings

Noble metal coatings such as gold, silver, rhodium, palladium, and platinum have been found to produce excellent DWC [2]. For example, Woodruff and Westwater [3] studied DWC of steam on electroplated gold surfaces and found that a minimum thickness of 200 nm of gold was required to obtain perfect dropwise condensation; otherwise film and dropwise condensation would coexist. A similar study for elec-

troplated silver was conducted by O'Neil and Westwater [4]; they concluded that the life-time of using silver as a DWC promoter depends on the plating thickness, composition and the base metal preparation. It is noted that the dropwise characteristics of these noble metals as DWC promoters have been controversial. Bernett and Zisman [5] showed that pure water spontaneously wets noble metals which are free of organic or oxide contaminations. Theoretically, noble metal materials have higher surface energy than oils and should not exhibit DWC. However, DWC have been found when using gold as the promoter, indicating that carbon (or organics) was probably the actual promoter. Woodruff and Westwater [6] have shown that the hydrophobicity of gold relates to the carbon to gold ratio on the surface. Thus, the heat transfer coefficient of DWC on noble metal surfaces depends on the coating methods and the operating environmental conditions.

2.1.3 Thin-layer Organic Coatings

Since the 1980s, thin-layer organic coatings with low surface energies have received more attention. For organic coatings, three factors are important to promote DWC. First, there must be a good, long-term adhesion between the coatings and metal substrates. However, it is well known that organic materials are more difficult to be sustained on metal substrates at elevated temperatures. Second, in general, the thicker the coating, the better its resistance to oxidation and erosion. However, the thickness of organic coatings cannot be larger than a few micrometers due to their low thermal conductivity; otherwise, the increase in heat transfer coefficient will be compensated by the increased thermal resistance of the coating itself [7]. Finally, if

the coating materials gradually peel off during DWC, it may contaminate the heat exchanger system and lead to other serious, unknown problems. Nevertheless, development of ultra-thin and stable coatings for DWC are still of interest to researchers.

Holden *et al.* [8] evaluated 14 polymer coatings for their ability to promote and sustain DWC of steam at atmosphere pressure. Nine of the coatings employed a fluoropolymer as a major constituent, four employed hydrocarbons and one, silicone. Six of these coatings were selected for applications to perform a heat transfer evaluation. Test results indicated that the steam-side heat transfer coefficient can be increased by a factor of five to eight through the use of polymer coatings to promote DWC.

Ma *et al.* [9] coated ultra-thin polymers, which were created by plasma polymerization and dynamic ion-beam mixed implantation (DIMI) method, on vertical brass tubes and conducted heat transfer experiments. It was concluded that, while the heat transfer enhancements were as high as 20 times, the promotion and the adhesion of the ultra-thin film with the substrate were strongly dependent on the process conditions of the two methods, which requires further study to optimize the performance. They later conducted a lifetime condensation test using this DIMI technique[10]. The discontinuous experimental results demonstrated that one surface had sustained DWC for about 1000 hours. The condensation heat transfer characteristics tended towards stability. In addition, the experiments proved that a polymer film prepared by the dynamic ion-beam mixed implantation (DIMI) method had good adhesion with the metal substrate. In 2002, Ma *et al.* [11] in-

vestigated the influence of processing conditions of polymer films by means of the DIMI technique on dropwise condensation heat transfer. The experimental results indicated that heat flux was increased up to 4.6 times and condensation heat transfer coefficient by 28.6 times of film condensation values for the brass tubes treated with various conditions. The surface processing condition was crucial to the adhesion between polymer film and metal substrate; different substrate materials require different optimal processing conditions, leading to different condensation heat transfer characteristics.

Taniguchi and Mori [12] studied the effectiveness of composite copper/gra-phite fluoride platings for promoting dropwise condensation of steam. It was confirmed that dropwise condensation occurs on the platings. Despite their exceptionally strong "water repellency" in an ordinary sense, they found no reduction, using the composite platings in place of conventional promoters, in the critical departure size of condensate drops. A hypothetical explanation was made on the apparent inconsistency between the manner of water-to-plating contact in the air and that in a condensing steam.

Zhao *et al.* [13] studied the DWC of steam by three layers of barium stearate monomolecular film on the copper plate (30 mm in diameter) using a Langmuir-Blodgett (LB) film balance. Perfect DWC was formed on the surface in laboratory conditions. However, it is well-known that surface films formed by means of a LB balance are unstable due to its weak physical interactions with the original substrate [14].

Recently, Das *et al.* [15, 16] applied an organic Self-Assembled Monolayers

(SAMs) coating to promote dropwise condensation of steam on horizontal tubes. The coating was created with SAMs on gold, copper and copper-nickle alloy surfaces. The monolayers were formed by chemisorption of alkylthiols on these metal surfaces. When compared to complete film condensation, the coatings increased the condensation heat transfer coefficient by factors of three to fourteen for different substrates under various conditions. The reason for using SAMs as DWC promoters is that SAMs formed by adsorption of hexadecylthiol [$CH_3(CH_2)_{15}SH$] on tube-metal surfaces creates a hydrophobic surface and hence should have DWC characteristics. The physio-chemical interactions between alkylthiol and metal are stronger than the physical interactions by means of the LB balance [14]. The condensing surfaces prepared by these SAMs were strong and lasted over a long period of time. In addition, being only monomolecular thick (1.0–1.5 nm), these coatings provide negligible heat transfer resistance, and the total amount of coating material involved is minuscule to pose any contamination problem should it peel off. Therefore, it was concluded that self-assembled monolayers appears to offer a strong potential for long-term DWC promoters, although durability tests have not been performed.

2.2 Self-Assembled Monolayers (SAMs)

2.2.1 Self-Assembly Systems

Self-assembly is the spontaneous organization of molecules or objects into stable, well-defined structures by noncovalent forces [17, 18]. The key idea in self-assembly is that the final structure is close to or at thermodynamic equilibrium; therefore,

it tends to form spontaneously and to reject defects. Self-assembly often provides routes to structures having greater order than can be reached in non-self-assembling structures. The final structure is predetermined by the characteristics of the initial subunits: the information that determines the final structure is coded in the structures and properties of the subunits (e.g., shapes and surface functionalities). Various strategies of self-assembly have been developed and employed to fabricate two- and three-dimensional structures with dimensions ranging from molecular to macroscopic sizes [19, 20, 21, 22, 23].

Self-Assembled Monolayers (SAMs) are the most widely studied and best developed examples of nonbiological, self-assembling systems [24, 25]. They are close-packed, ordered, and long-chain organic molecular assemblies that are spontaneously formed on the surfaces of appropriate substrates by the adsorption of amphifunctional molecules. One part of these assemblies has a specific strong affinity for the surface and the other part has very weak affinity or none [26, 27]. The interactions between molecules and substrates, generally a chemical bond, result in a pinning of the headgroup to a specific site on the substrate surface.

2.2.2 Self-Assembled Monolayers (SAMs) on Gold

The phenomenon of spontaneous adsorption of alkanethiolates [$X(CH_2)_nSH$] on gold was first discovered by Nuzzo and Allara [28]. This intriguing behavior has been reexamined in numerous studies. To date, it has been established that surface-active organosulfur derivatives have a strong affinity to many metals due to the formation of multiple bonds with surface-metal clusters. Besides gold, it has been

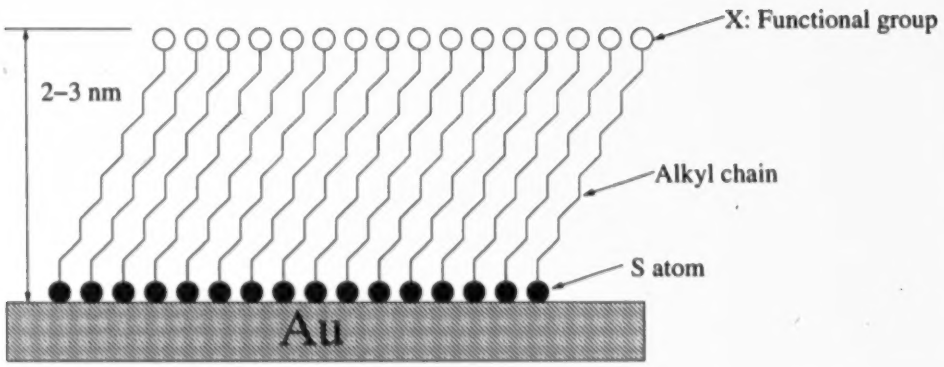

Figure 2.1: Schematic of a highly ordered monolayer of alkanethiolate formed on a gold surface.

found that organosulfur compounds could coordinate strongly to silver [29], copper [29, 30, 31], platinum, mercury [32], and iron [33].

Although gold is generally considered as a chemically inert element, which resists atmospheric contamination, it has a strong specific interaction with organosulfur compounds. In fact, the monolayers of alkanethiolates on gold are the best characterized systems of SAMs to date.

A schematic of a highly ordered monolayer of alkanethiolate formed on a gold surface is shown in Figure 2.1. This process is believed to involve an oxidative addition of an S-H bond to the gold surface, followed by a reductive elimination of the hydrogen:

$$X(CH_2)_nSH + Au^0 \longrightarrow X(CH_2)_nS^-Au^+ \cdot Au_n^0 + 1/2H_2 \qquad (2.1)$$

While some debate still remains on the reaction mechanism, one conclusion has

been reached unanimously; i.e. the chemisorbed species on gold is a thiolate type [34]. Sulfur atoms bonded to the gold surfaces bring the alkyl chains into close contact; these contacts freeze out configurational entropy and lead to an ordered structure. It is noted that the sulfur/Au interaction is purely physiochemical and not by means of a covalent bonding [27], contrary to that claimed elsewhere [15].

The structure and properties of SAMs from alkanethiolates on gold have been examined using a number of techniques [27]. It is generally accepted that sulfur atoms form a $(\sqrt{3}\times\sqrt{3})R30^0$ overlayer on the Au(111) surface (See Figure 2.1) and that these systems are heterogeneous and structurally complex: The alkyl chains may form a "superlattice" at the surface of the monolayer; that is, a lattice with a symmetry and dimension different from that of the underlying hexagonal lattice formed by sulfur atoms. These indicate that the order in the top part of SAMs is not dictated solely by the sulfur atoms directly bonded to the gold surface, but also depends strongly on the intermolecular interactions between the alkyl backbones. For carbon chains of up to approximately 20 carbon atoms, the degree of interaction in a SAM increases with the density of molecules on the surface and the length of the alkyl backbones. Only alkanethiolates with $n > 11$ form closely packed and essentially two-dimensional organic quasi-crystals supported on gold [27]. When alkanethiolates are terminated in a head group other than methyl, it becomes even more complicated to predict and determine the structures of SAMs.

SAMs of alkanethiolates on gold exhibit many features that are most attractive about self-assembled systems [27]: ease of preparation, low density of defects, good stability under ambient laboratory conditions, and amenable to control interfacial

properties (i.e. wettability). As an example, if the end functional group is methyl [$-CH_3$], the surface exhibits hydrophobic characteristics with water having contact angles between 110–118° [35, 36]. If the end group is selected as carboxylic acid [$-CO_2H$], the surface would become hydrophilic having near zero contact angle for water. Furthermore, it has been experimentally verified [35] that long-chain thiols form films that are thermally more stable than those from shorter chains. For $n < 14$, the contact angle of water on the surface composed of purely methyl groups is progressively lower with decreasing chain length; for longer chain thiols, the wetting properties are largely independent of chain length.

2.2.3 Self-Assembled Monolayers (SAMs) on Copper

Active metals such as copper and iron are more reactive to alkanethiolates and more sensitive to attributes of the alkanethiol than gold. The mechanism of formation of alkanethiol monolayers on these metals is similar to that on gold. Unfortunately, there are few studies focusing on the properties of alkanethiol adsorption on copper. The reason might be rationalized by the difficulties in obtaining reproducible and high-quality SAMs on copper [37].

Copper surfaces readily form oxides that adsorb polar contaminants. Slightly oxidized surfaces of copper are subject to the chemisorption of alkanethiols; however, the formed monolayers differ in structure and properties from those formed on absolutely oxide-free surfaces. It is likely that the monolayer could form on a roughened copper/copper-oxide interface and this monolayer might be heterogeneous in structure [37]. Therefore, to obtain reproducible and high-quality mono-

layers on copper, the copper surfaces should be clean and oxide-free. Oxygen must be completely excluded throughout the preparation procedures [38]. Occasionally, copper films manufactured even under oxygen-free conditions did not result in high-quality monolayers [38].

Vogt *et al.* [39, 40] used an electrochemical polishing method to obtain an oxide-free copper surface. This sample treatment included electrochemical polishing at 4 V in 66% orthophosphoric acid for a few seconds, rinsing with Millipore water and followed by polishing again at 1.8-2.4 V for 10 s. This treatment is similar to that of Kruft *et al.*, who performed electrochemical polishing in 50% orthophosphoric acid at 2-2.4 V for 1 minute to eliminate the oxide. Later, Vogt *et al.* [40] modified their previous procedures by immersing the copper in 1 mM HCI for 5-10 minutes after electrochemical polishing to obtain an oxide-free surface. However, it was suggested that chloride ions might adsorb on the copper surface, which would reduce the surface activity for adsorption [41].

Recently, Fent *et al.* [42] proposed a new method for copper treatment by etching the polished copper surface in 7 M HNO_3 for 3 s and evaluating the effects of surface treatment on the quality of monolayers using impedance measurements. Their results demonstrated that HNO_3 etching was the most efficient way to form high quality films.

2.2.4 Thermal Stability of SAMs

The application of SAMs to promote DWC of steam is largely dependent on the thermal stability of these organic thin films. The deterioration of alkanethiol SAMs

under thermal stress has been widely addressed in the literature. It has been found that SAMs could be stable within moderate temperature range. The deterioration of SAMs by thermal stress will result in the loss of order in the monolayers [37].

Nuzzo *et al.* [28] first demonstrated loss of sulfur from SAMs of hexadecanethiolate on gold over the temperature range of 150-200°C. Infrared (IR) results indicated that the thermal-induced structural changes were reversible below 125°C; however, these changes became irreversible when heated up to 150°C. Partial desorption of the adsorbate or structural restructuring might occur at 150°C. When the temperature was increased to near to 200°C, no adsorbate is left on the substrate. Differential scanning calorimetry (DSC) studies have also revealed that the thermal behavior of surface-adsorption molecules significantly differs from that of the bulk materials. Furthermore, the adsorption bond energy was estimated from thermal desorption results [43, 44].

In their later work, Nuzzo *et al.* [45, 46] performed a temperature-programmed desorption of methanethiolate SAMs on gold. It was reported that the desorption is a molecular process; i.e., there was no ionization involved in the desorption. In a detailed mass spectroscopic study, Jeffey and Madix [47] illustrated the desorption mechanism of a *tert*-butyl thiolate monolayer on gold. The *tert*-butyl thiolate is stable up to about 130°C and a maximum desorption is at about 200°C. In their opinion, the main decomposition might occur via a disproportion reaction between two adsorbed thiolate molecules in SAMs, resulting in a thiol molecule with one alkene, and adsorbed sulfur on gold. The formation of H_2S might be the result of a direct reaction of the thiol and adsorbed sulfur.

A STM/XPS study of dodecanethiol SAMs on gold showed surface phase changes accompanying the loss of thiolates [48]. It showed that no surface change occurred below 85°C. This STM/XPS study also revealed that desorption competed with thiolate oxidation and alkylsulfonates remained in the monolayer for temperatures lower than 100°C. At 100°C, the top layer of the gold mobilized and the depressions fused with terrace edges forming large domains, resulting in a lack of thiolate molecules.

Recently, Schlenoff *et al.* [49] reported that for 1-octadecanethiol SAMs on gold, a complete loss of sulfur occurred at 210°C. However, the desorption process occurred in a wide temperature range with partial loss at 100°C. In general, desorption increases and coverage decreases with increasing temperature.

2.3 Summary

Although DWC offers a strong potential to the industrial application for its much higher heat transfer coefficient, the key point has been, and still is, to develop reliable and long-lived DWC promoters. Using ultra-thin-layer organic coatings as DWC promoters has been the most attractive research area in the last two decades with the development of ultra-thin coating technique and new organic compounds.

Self-Assembled Monolayers (SAMs) were first used to promote DWC heat transfer by Das *et al.* [15, 16]. Although it was concluded that the heat transfer coefficient can be increased by different factors under different conditions, durability tests have not been conducted.

Based on previous work, it has been found that the mechanism of formation of

alkanethiol monolayers on copper and gold surfaces is similar, but the quality of SAMs on copper substrates is not as good as that on gold because copper surface oxidizes very quickly upon exposure to air. The structure of SAMs on copper is extremely sensitive to the history of sample and technique of sample preparation. Therefore, if DWC heat transfer coefficient depends on the structure of SAMs, it would be very difficult to obtain reproducible enhancement of DWC heat transfer coefficient when applying SAMs on copper as the promoters. Furthermore, this will make it impossible to characterize the changes of SAMs during condensation process.

The application of SAMs to promote DWC of steam is largely dependent on the thermal stability of these organic thin films under steam-blowing conditions, which has not been addressed in the literature.

Therefore, in this study, in order to have consistent experimental results, all condensation experiments were conducted on copper blocks to eliminate the effect of substrate material. The copper blocks were coated with an ultra-thin layer of gold to ensure that the same quality of SAMs can be obtained for each experiment. Octadecanethiol [$HS(CH_2)_{17}CH_3$] SAMs on these gold-coated -copper substrates were applied as DWC promoters. For comparison, 16-mercaptohexadecanoic acid [$HS(CH_2)_{15}COOH$] SAMs was used for film condensation. The choice of these SAMs allows a systematic surface energetic variation in relation to the enhanced heat transfer coefficient.

Chapter 3

Experimental Procedures

Condensation experiments were conducted on a vertical surface of a rectangular block (107.95 × 31.75 × 50 mm) of pure copper (oxide free electrolytic copper, obtained from the Department of Physics at the University of Alberta). A schematic of this copper block is shown in Figure 3.1.

3.1 Contact Angle Hysteresis

It is a well known experimental fact that most of the heat transfer in dropwise condensation occurs during the early stage of the formation and growth of a droplet. It must therefore be the aim of any pretreatment of the condenser surface to cause the condensate droplet to depart as early and as quickly from the condenser surface as possible. The departure of the drop is resisted by the adhesion of the droplet to the condenser surface, and the resistance is attributed to contact angle hysteresis [50, 51, 52, 53, 54].

Contact angle of an advancing droplet on a solid surface is different from that of a receding one. The difference between the advancing and receding contact angle is the contact angle hysteresis. It may be due to dynamic effects, but it also exists

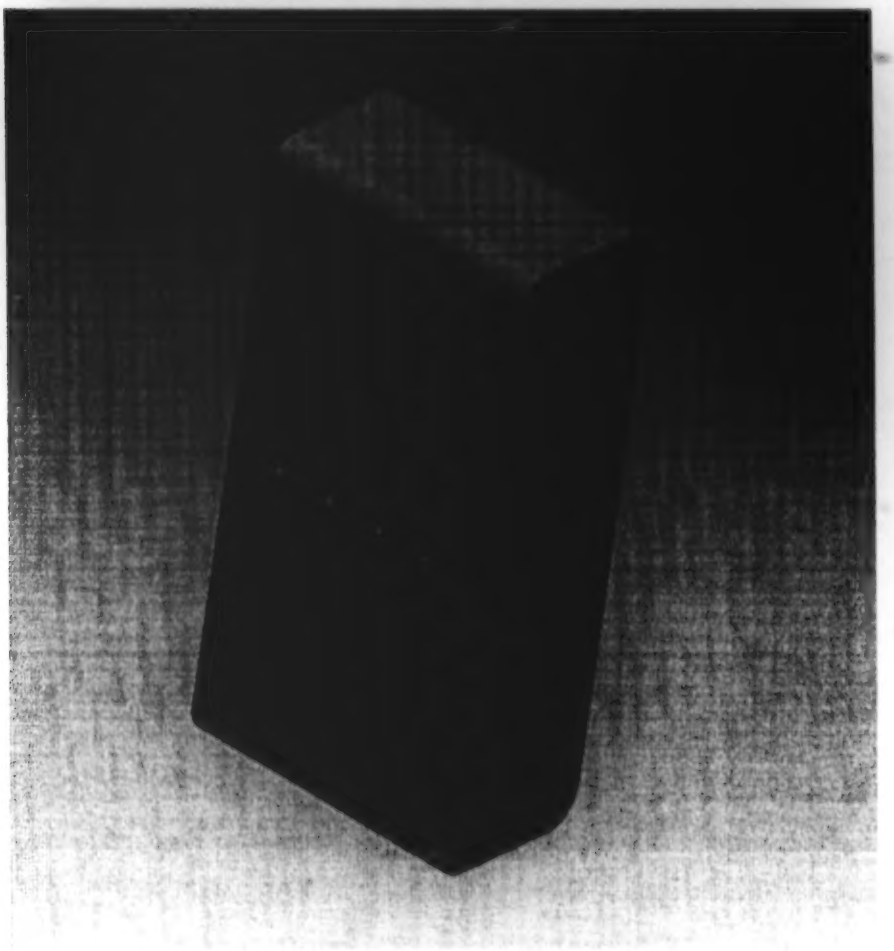

Figure 3.1: Schematic of the rectangular copper block.

under static conditions. The two main causes of static contact angle hysteresis are surface heterogeneity and roughness [55]. The effect of contact angle hysteresis on the departure of droplets from surface is readily illustrated by a raindrop on a dirty

window panel: an adhering water droplet will show a relatively large contact angle hysteresis, due to roughness and heterogeneity. On the other hand, a water droplet on a smooth and homogeneous paraffin surface (such as certain plantar leaves) will show little contact angle hysteresis and the water droplet will run off readily. Thus, in order to reduce the resistance to drop removal in dropwise condensation heat transfer, the heterogeneity and roughness of the condenser surface should be made as small as possible.

It has been found experimentally [56, 57, 58, 59] that the size and distribution of the condensed droplets have a large effect on the heat transfer efficiency; the smaller the droplet (less than 100 μm in diameter), the higher is the heat transfer coefficient [59]. An analytical expression for the limiting size of a drop to slide on

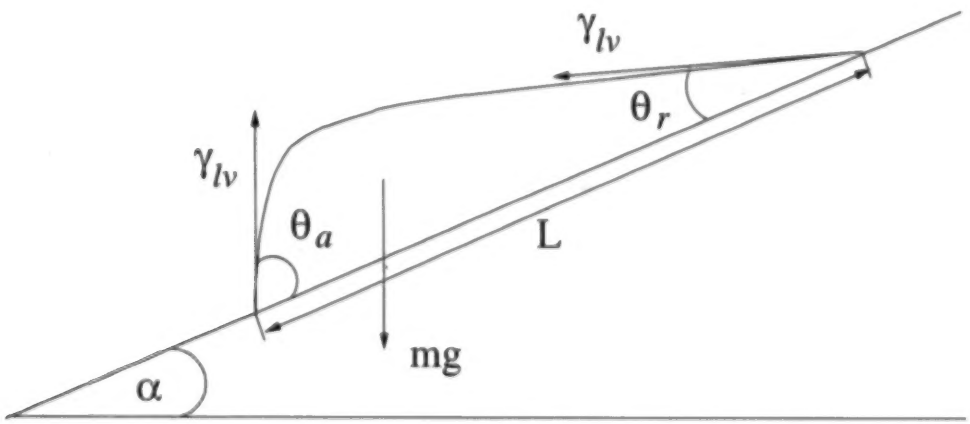

Figure 3.2: Profile of a drop on an inclined surface.

an inclined surface is given by [50]

$$mg \cdot \sin\alpha = \gamma_{lv} \cdot (\cos\theta_r - \cos\theta_a) \tag{3.1}$$

Equation 3.1 strictly applies to a drop of cylindrical symmetry with the cylinder axis normal to the paper, as shown in Figure 3.2. Here θ_a represents an advancing contact angle and θ_r a receding contact angle. Sliding of the drop is initiated when the limiting contact angle θ_a' and θ_r' are reached while the angle of inclination α is increased, at constant mass of the drop m. Alternatively, at constant inclination, the drop may grow, accompanied by changes in θ_a and θ_r until it reaches a critical mass m', at which the contact angle assume their critical values θ_a' and θ_r', and sliding starts. This qualitatively describes the behavior of real droplets on inclined surfaces. Obviously, the limiting mass m' for drop removal will decrease with decreasing contact angle hysteresis. Therefore, the condensing surfaces should be carefully perpared to eliminate the effects of contact angle hysteresis before condensation experiments.

3.2 Sample Preparation

3.2.1 Condenser Surface Polishing

In order to reduce contact angle hysteresis due to roughness, the condensing surfaces were polished manually according to the following procedures for lapping, polishing and fine polishing:

1. Lapping: The copper block of interest was put onto a lapping machine (Lapmaster) using a 5 μm grit size alpha aluminum powder (E.T. Enterprises)

suspended in mineral oil and varsol or portable heater fuel (Imperial Oil) until the entire surface appeared to be smooth. It was then rinsed thoroughly with ethanol and water in order to remove the oil and all coarse grains of the polishing compound.

2. Polishing: The above cleaned and smooth surface was polished by means of a high speed brass polishing wheel. The first step is to employ a Nylon polishing cloth (Buehler ltd.) using a 6 μm grit size diamond polishing compound (Hyprez) and a Diamet fluid (E.T. Enterprises). This was followed by cleaning the block with ethanol for removal of the oil used. The next step is to employ a pellon polishing cloth (E.T. Enterprises). The polishing grade is a 1 μm Diamet diamond suspension (E.T. Enterprises). This process removes large scratches left from lapping and last step, and results in a highly reflective surface. Before moving onto the next procedure, the copper block was cleaned in an ultrasonic cleaner filled with deionized ultra filtered (DIUF) water (Fisher Scientific) for 15 minutes.

3. Fine Polishing: Fine polishing was conducted on a micro-polishing cloth (E.T. Enterprises) using a relatively slower rotating brass polishing wheel. A 0.3 μm and subsequently a 0.05 μm grit size of aluminum oxide powder (Beta Diamond Products Inc.) suspended in DIUF water were used as the polishing grade. Between each fine polishing steps, the block was rinsed with DIUF water, methanol and acetone (Fisher Scientific) to remove possible traces of organic materials.

In order to avoid finger oil contamination on the copper block, during the entire preparation, the copper block were only handled with textured chlorinated powder free latex medical examination gloves (Fisher Scientific). The final polishing produced surfaces that are virtually similar to those of a mirror finish. The roughness of these surfaces is in the order of around 50 nm. The copper block was then kept in a chemical-resistant vacuum desiccator (Fisher Scientific) to prevent contamination from surroundings until the next preparation step.

3.2.2 Thermal Evaporation

After polishing, a titanium and subsequently a gold layer were coated onto the condensing copper surface by a vacuum vapor deposition technique. Here, the thin layer of titanium is called a "glue layer", which serves as an adhesion promoter between the substrate (copper) and gold [60]. The thickness of titanium and gold are 15 and 100 nm, respectively; hence, their heat transfer resistances are negligible comparing with that of the copper block (50 mm thick).

Preparation of these coatings is described by the following procedures: the polished copper blocks were placed in a diffusive-pumped vacuum chamber where $\sim$ 15 nm of titanium (99.9995%, Kurt J. Lesker Co.) and $\sim$ 100 nm of gold (99.999%, Kurt J. lesker Co.) were sequentially evaporated from tungsten holders onto the copper blocks at a maximum evaporation rate of $\leq$ 0.2 nm/sec and a pressure of $\leq 2 \times 10^{-6}$ torr. Deposition rates and mass thickness were monitored using an Infinicon XTM/2 quartz crystal monitor. After evaporation, the chamber was cooled down for half an hour and then slowly backfilled with air. The coated

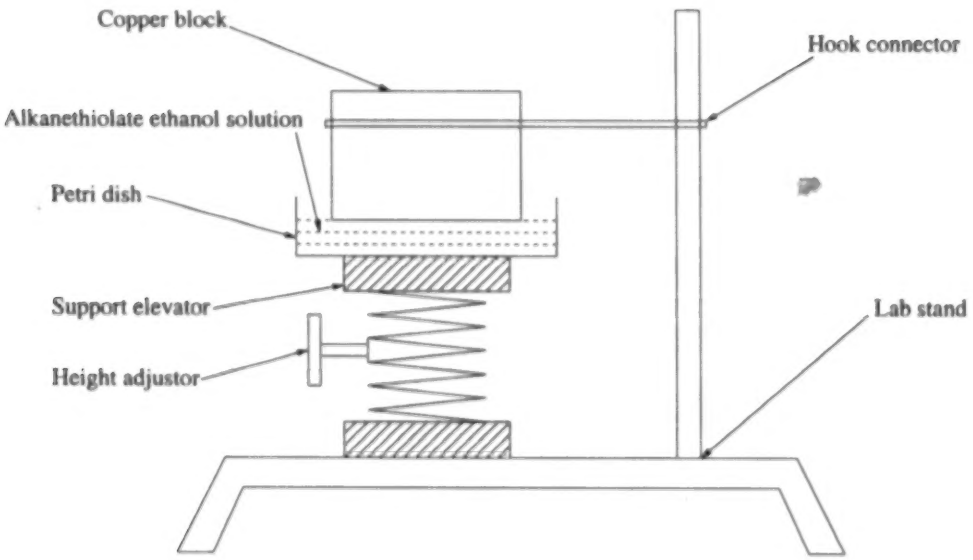

Figure 3.3: Schematic of the deposition of alkanethiol SAMs on a copper surface.

copper blocks were removed immediately for monolayer assembly, similar to those prepared elsewhere [36].

3.2.3 Deposition of SAMs

Immediately after being taken out from the chamber, the copper blocks were thoroughly rinsed with ethanol and dried with a nitrogen jet. The blocks were then made in "contact" with either a 5 mM 1-octadecanethiol or 16-mercapto-hexadecanoic acid ethanol solutions for one hour. The alkanethiolate ethanol solutions were prepared by dissolving 1-octadecanethiol and 16-mercapto-hexadecanoic acid (Aldrich) in 100 % ethanol (the Chemistry Department at the University of Alberta) and kept in a sealed flask overnight before use. Typically, SAMs are

formed by immersing the entire surface into the alkanethiol solution [36]. However, it was found that this procedure does not produce good structure of SAMs, as indicated by fourier transform infrared (FT-IR) results. This poor structure can lead to erroneous interpretation of condensation data. Although the reason for this is unclear, it was found that placing a copper block upside down and allowing only the condenser surface to be in contact with the alkanethiolate solution (See Figure 3.3) produces good quality of SAMs which are comparable with those in the literature [35, 36]. After SAMs formation, the samples were rinsed sequentially with ethanol and DIUF water, and blown dry with nitrogen before use.

3.3 Experimental apparatus

3.3.1 Fourier Transform Infrared Spectroscopy (FT-IR)

The quality of SAMs before and after the condensation experiments was detected using a fourier transform infrared spectroscopy (Nexus 670, Thermo Nicolet). A Pike VeeMax accessory with a grazing angle of 75° from the surface normal and a polarizer set to 90° so as to minimize light scattering from the surface were used. The reflected infrared signal was detected using a liquid N_2 cooled MCT-A detector. The spectra resolution was set to 0.964 cm^{-1} for the data collection and 512 scans were collected in order to increase the signal-to-noise ratio. An infrared gain of 2 was selected for all reflectance infrared measurement to ensure that the input infrared signals are constant. The spectra were referenced to the bare gold substrate which was prepared according to the same polishing and evaporation procedures.

3.3.2 Spectroscopic Ellipsometry

The variation of SAMs thickness during the condensation experiments was determined using a variable angle spectroscopic ellipsometry (GESP5, Sopra). The ellipsometry measurements were taken by linear polarizing a beam of light from a 75W Xe-arc lamp using a polarizer rotating at 8 Hz and directing onto the surface at a 75° angle from the surface normal. The data for $\tan\Psi$ and $\cos\Delta$ were collected over a visible light range (300–850 nm) using a rotating analyzer in a current tracking mode [36]. The $\tan\Psi$ and $\cos\Delta$ parameters were collected for the bare Au/Ti/Cu surface as a reference before the monolayers were formed, and a new set of $\tan\Psi$ and $\cos\Delta$ curves were measured again using an ambient-film-substrate model for regression with known optical constant (n and k) for SAMs/Au/Ti/Cu surface. The refractive index for SAMs/Au/Ti/Cu surface as a function of wavelength was independently obtained from a Sopra GXR grazing X-ray reflectometer, rather than assuming an index of refraction (e.g., $n = 1.46$) at a given wavelength (e.g., $\lambda = 63.28$ nm) as typically performed in the literature. Such spectroscopic measurements are expected to provide more accurate results in ellipsometer thickness since the optical constants for a range of wavelength were used simultaneously. The thickness was calculated according to the following equation:

$$(\tan\Psi)e^{(i\Delta)} = f(n_i k_i t_i) \tag{3.2}$$

where n and k are the optical constants of the film and t is its thickness; the subscript i represents different wavelength. The averages of three measurements made at each location on the surface were used to calculate the thickness of each

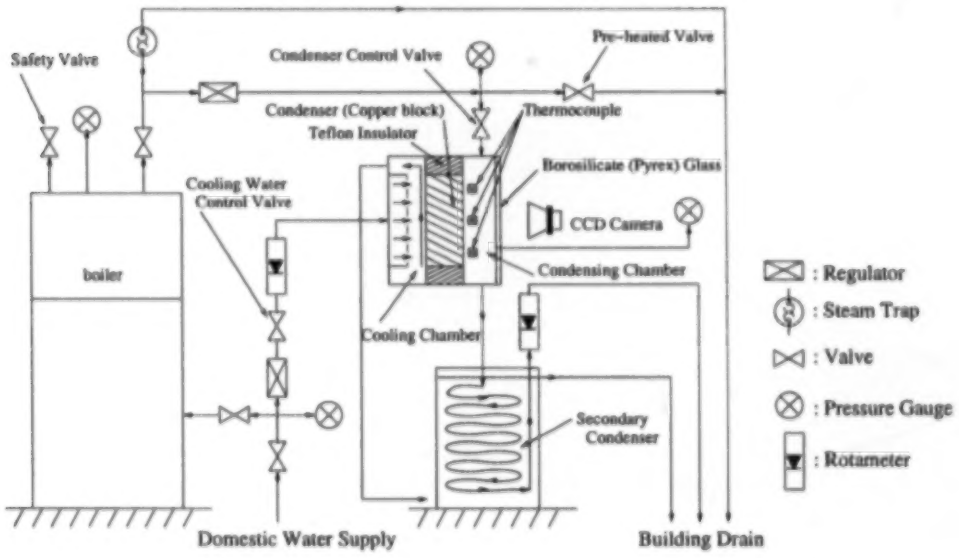

Figure 3.4: Schematic of an experimental set-up for the measurements of the condensation heat transfer coefficient.

sample.

3.3.3 Experimental Set-up

Figure 3.4 shows schematically the experimental set-up for the measurements of condensation heat transfer coefficient. Steam is generated by a hot shot electric steam boiler (Automatic Steam Products Corporation, NY), which is filled automatically with domestic water supply from the building. As shown in Figure 3.4, steam flows through a stainless steel tubing, regulator and condenser control valve before entering a condensation test assembly where condensation happens on the SAMs/Au/Ti/Cu surface and condensation heat transfer coefficients are measured.

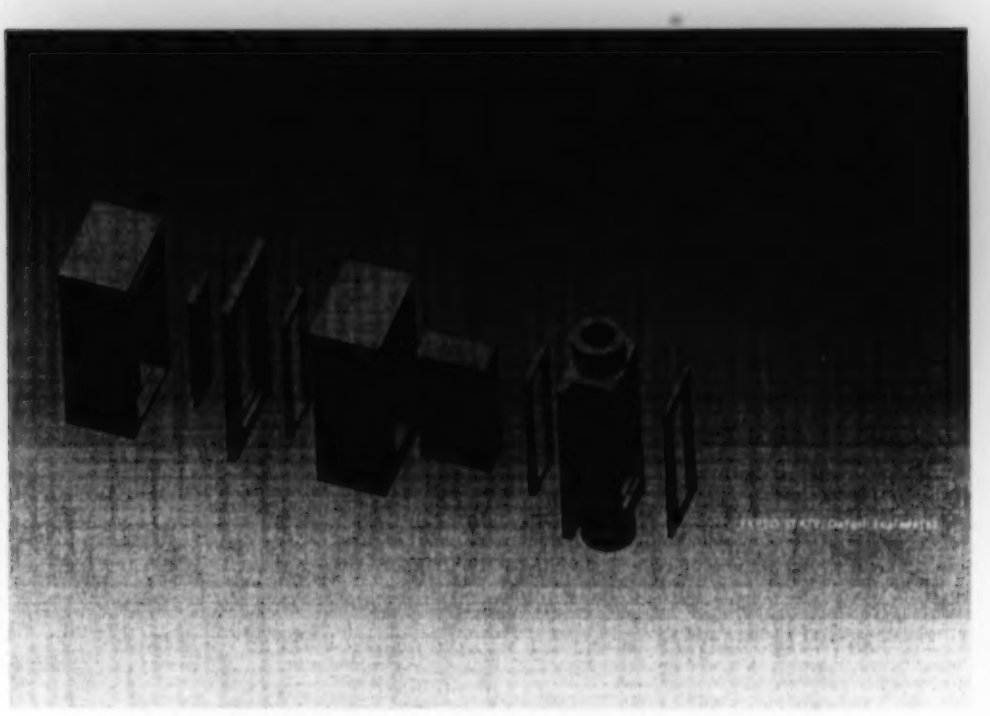

Figure 3.5: An exploded view of the condensation test assembly.

The condensation test assembly is shown in more detail with an exploded view in Figure 3.5 obtained by Pro/ENGINEER Wildfire.

A steam trap was used to separate the condensed liquid steam in the flowing process. All condensate and excess steam which did not condense in the test assembly was passed through a secondary condenser and then the flow rate was measured with a standard glass tube flowmeter (Omega). The secondary condenser was designed to condense all remaining steam, so that the mass flow rate of the condensate water will be the same as that of the steam passing through

the condensing chamber. Combining this with the cross-sectional area and condensation pressure measured from a pressure gauge in the condensing chamber, a steam velocity passing through the condensing surface can be calculated according to equation 3.3 [61]:

$$\dot{m} = \int_s \rho v dA \tag{3.3}$$

where v is the steam velocity, $\dot{m}$ is the mass flow rate, ρ is the saturation steam density, and A is the cross-section area of condensing chamber.

The height of the flowmeter was calibrated and labeled before all condensation experiments as it would alter the pressure inside the condensing chamber. It is noted that the condensation pressure P_{steam} is the sum of the atmosphere pressure P_{atm} and gauge pressure P_{gauge} and that adjustment in the condenser control valve can increase both the steam velocity v and gauge pressure P_{gauge}. By adjusting the condenser control valve and height of the flowmeter, an expected condensation pressure and steam velocity can be obtained. For example, when atmosphere pressure increases, condensation pressure will increase accordingly while the gauge pressure will not change to maintain constant steam velocity. By lowering the flowmeter, the gauge pressure will decrease. Thus, the condensation pressure and steam velocity will remain constant no matter how the local atmosphere pressure changes. Alternatively, if the condenser control valve is increased while atmosphere pressure remains unchanged, the steam velocity will increase. Condensation will happen at a higher steam pressure because the gauge pressure also increases. By lowering the flowmeter again, the gauge pressure will decrease to ensure that the condensation experiment is conducted at the same steam pressure but in a higher

steam velocity. In this study, the condensation pressure is set to be standard atmosphere pressure (101.325 kPa). A higher, but constant, steam velocity (6.13 m/s) was used in order to eliminate the effect of non-condensible gas [62].

Domestic water from the building was also used as the coolant. To ensure a steady flow for the cooling system, the coolant water first passed through a regulator where the exit pressure was maintain constant. The flow rate was adjusted through a cooling water control valve to obtain the expected heat flux by monitoring a glass tube full-view flowmeter (Brooks Instrument). After flowing through the cooling chamber and secondary condenser, the coolant water is drained with the condensate of the system.

3.4 Measurement Principle

Figure 3.6 shows a schematic of the measurement system for the copper block condenser. Two assumptions were made in the calculations:

1. One-dimensional steady-state conduction heat transfer along the "X" direction was assumed. The copper block was insulated by a thick Teflon (PTFE) block and two Teflon rings from the surroundings (as shown in Figure 3.5), so that heat loss in other directions could be neglected.

2. The thermal conductivity of the copper block was assumed constant in each region of δ_0, δ_1, δ_2, and δ_3 which depend on the temperatures T_1, T_2, T_3, and T_4, respectively. The relationship between thermal conductivity of copper and temperature can be obtained by polynomial regression, as shown in Fig-

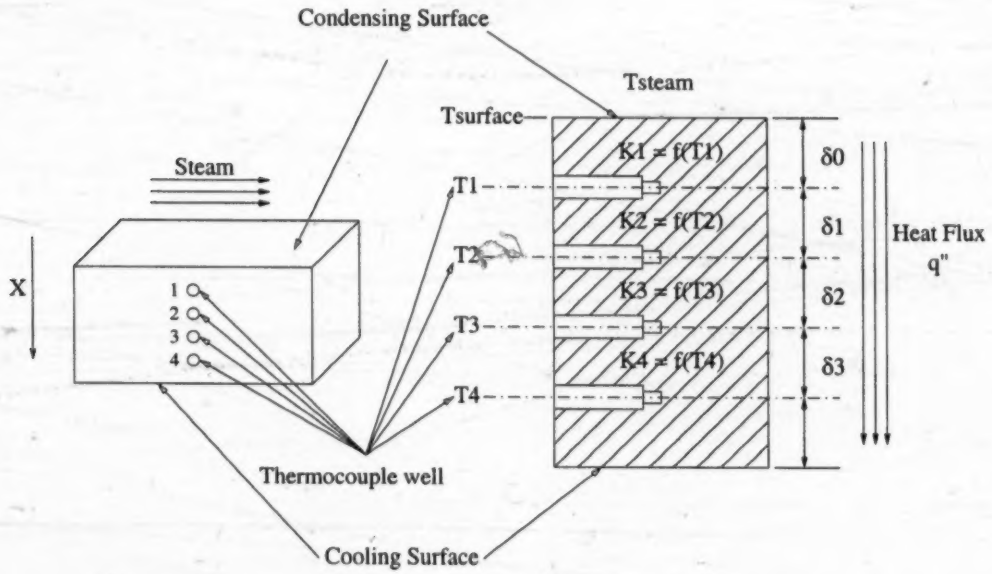

a: Rectangular Copper Block Condenser

b: Right Section View

Figure 3.6: Schematic of the measurement system of the copper block condenser.

ure 3.7. The polynomial curve-fitting coefficients will be used for calculation in this study.

To verify these two assumptions, a finite element model was set up to simulate the heat transfer process through ANSYS 7.0. Boundary conditions of this model were: heat flux of the surfaces area which contact with teflon were set to be zero; surfaces which contact with the steam and cooling water were set to be at a constant temperature; thermocouple wells were assumed to cylinders filled with air. The thermal conductivity of air is also temperature-dependent and curve-fitting

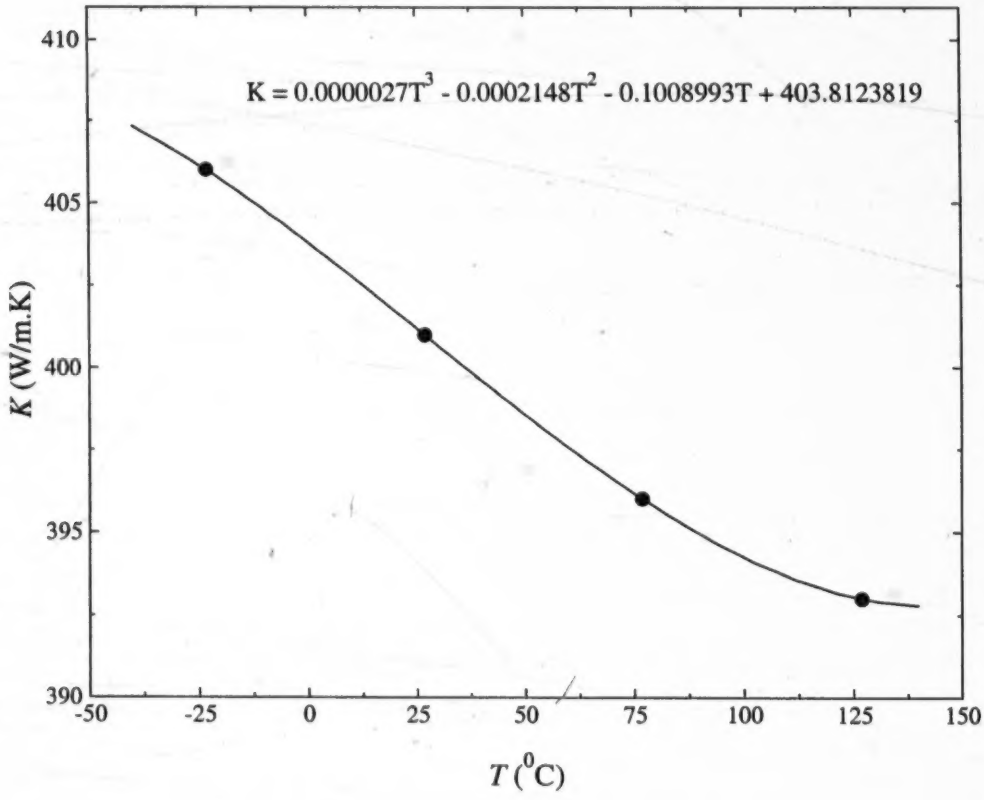

Figure 3.7: Polynomial regression curve-fitting of copper thermal conductivity.

coefficients were obtained by polynomial regression as copper (see Figure 3.8). The simulation results are shown in Figure 3.9. It can be seen that temperature gradient of the copper block center line is nearly linear. Therefore, a heat transfer coefficient can be determined from the following relationships:

$$h = \frac{q''}{T_{steam} - T_{surface}} \tag{3.4}$$

Table 3.1: Calibration values of the four thermocouple probes.

$T_{standard}$ (°C)	T_1 (°C)	T_2 (°C)	T_3 (°C)	T_4 (°C)
31.92	31.19	31.14	31.11	31.11
39.19	38.34	38.28	38.27	38.26
46.38	45.49	45.43	45.42	45.41
52.22	51.40	51.32	51.32	51.31
58.16	57.46	57.39	57.38	57.36
63.71	62.92	62.85	62.85	62.83
68.63	67.67	67.62	67.61	67.59
76.83	75.63	75.59	75.58	75.55
82.04	80.80	80.76	80.75	80.73
89.21	87.97	87.92	87.91	87.89
96.23	95.03	94.98	94.98	94.96
103.41	102.32	102.32	102.30	102.28

and

$$q'' = -K \cdot \frac{dT}{dX} \tag{3.5}$$

where the heat flux q'' was obtained by averaging the heat flux through the copper block

$$q'' = \frac{1}{3} \cdot (K_2 \cdot \frac{T_1 - T_2}{\delta_1} + K_3 \cdot \frac{T_2 - T_3}{\delta_2} + K_4 \cdot \frac{T_3 - T_4}{\delta_3}) \tag{3.6}$$

and the mean temperature of the condensing surface $T_{surface}$ was calculated by extrapolating the temperature profile from the copper block

$$T_{surface} = T_1 + \frac{q''}{K_1} \cdot \delta_0 \tag{3.7}$$

Thus, only the following five temperatures (T_1, T_2, T_3, T_4, and T_{steam}) and four distances (δ_0, δ_1, δ_2, and δ_3) are experimental quantities.

Table 3.2: Calibration values of the three thermocouple wires.

$T_{standard}$ (°C)	T_{steam1} (°C)	T_{steam2} (°C)	T_{steam3} (°C)
99.03	97.95	97.88	97.91
100.62	99.60	99.53	99.55
102.04	101.05	100.97	101.00
103.45	102.49	102.43	102.45
104.62	103.64	103.56	103.58
106.41	105.33	105.25	105.27
107.98	106.84	106.78	106.79
110.03	108.86	108.78	108.78

The temperatures T_1, T_2, T_3, and T_4 were determined by inserting four Type T (copper vs. copper-nickel) miniature quick disconnect small diameter thermocouple probes (Wika Instruments Ltd., Edmonton) into thermocouple wells of the copper block (see Figure 3.6). The spacings between these thermocouple probes (0.508 mm diameter) and tips of the thermocouple well (0.635 mm diameter) were filled with a thermal compound (Wakefield Engineering Inc.) to ensure perfect contact between the thermocouple probes and copper block. T_{steam} was measured by three Type T thermocouple wires (Minco Products Inc.) mounted into the condensing chamber. This value of T_{steam} was compared with the saturation temperature corresponding to the condensing steam pressure obtained by the pressure gauge connected to the condensing chamber (see Figure 3.4).

It is noted that maximum error of Type T thermocouple is 1°C, which is too large for this study. Therefore, all thermocouples were calibrated in a variable temperature oil bath (Model 910AC, Rosemount Engineering Co.) against a thermometry system (2189A, Fluke), which consists of a 2180A digital thermometer (with microcomputer Type 2) and a Y2039 resistance temperature probe. Cali-

Table 3.3: Factors that affect the maximum error of temperature measurements.

No.	Factor	Error (°C)
1	Resolution of the digital thermometer	0.01
2	Maximum system error of the thermometry system	0.16
3	Confidence limits (99%) of the DAS output	0.03
4	Maximum error due to the calibration coefficients	0.20
Maximum errors of all thermocouples		0.26

bration values of the four thermocouple probes and three thermocouple wires are shown in Tables 3.1 and 3.2, respectively. Calibration coefficients for each thermocouple were obtained by the second order of polynomial regression, which can reduce the maximum error down to 0.20°C (see Table 3.3). Figures 3.10 and 3.11 show the calibration curves of all thermocouples. These calibration coefficients were input into a data acquisition system (DAS), which includes a PCI-DAS-TC board (Measurement Computing Corp.) and a computer with a data acquisition software (LabView). Table 3.3 shows all the factors that effect the system error during calibration process. By a Root-Sum-Square criterion [63], the maximum error of these thermocouples is reduced to 0.26°C after calibration and a relative maximum error is less than 1%.

After the thermocouple wells were drilled, the exact distances (δ_0, δ_1, δ_2, and δ_3) were measured by a Leitz universal toolmaker microscope (Model UMW, Leitz Wetzlar). Table 3.4 shows all the factors that effect the maximum error during the measurement process. It can be seen that, by a Root-Sum-Square criterion, the maximum error is controlled to be less than 0.09 mm. Comparing with the height of copper block (50 mm), having a relative maximum error of less than 1% is

Table 3.4: Factors that affect the maximum error of distance measurements.

No.	Factor	Error (mm)
1	Resolution of the microscope	0.001
2	Maximum error due to spacings between thermocouple well and thermocouple probe	0.064
3	Confidence limits (99%) of the distance measurement	0.030
4	Maximum error due to angle bias (less than 1°) of drill	0.044
Maximum errors of δ_0, δ_1, δ_2, and δ_3		0.083

indeed excellent for this study. The measurement distances δ_0, δ_1, δ_2, and δ_3 were then input into the data acquisition system to calculate heat transfer coefficients.

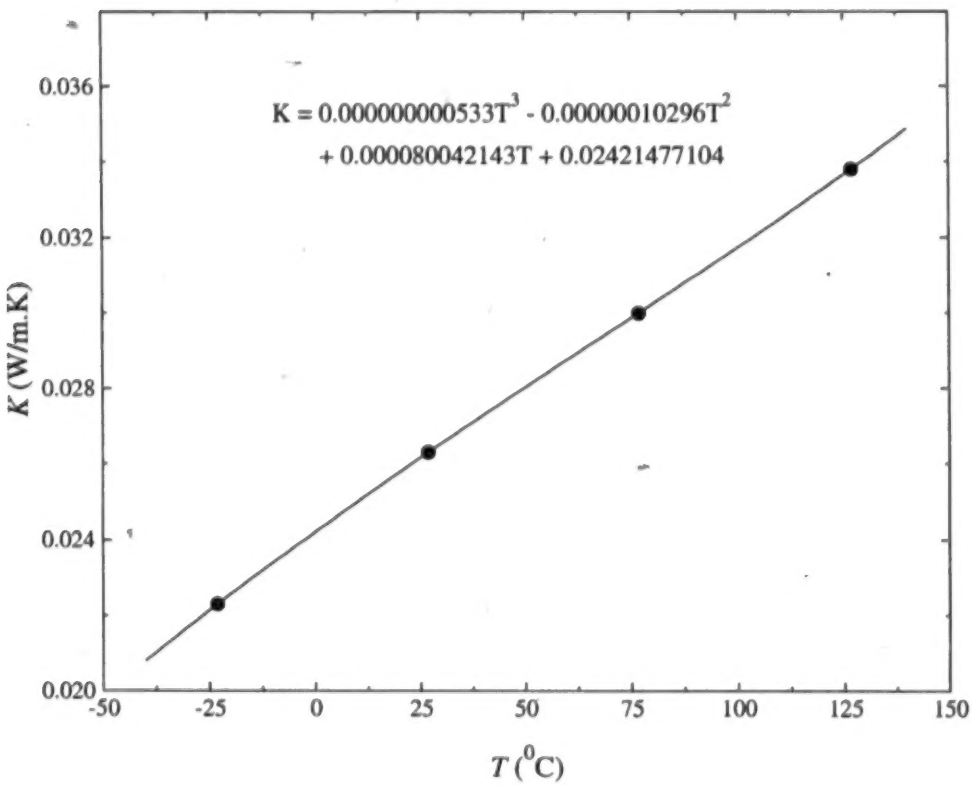

Figure 3.8: Polynomial regression curve-fitting of air thermal conductivity.

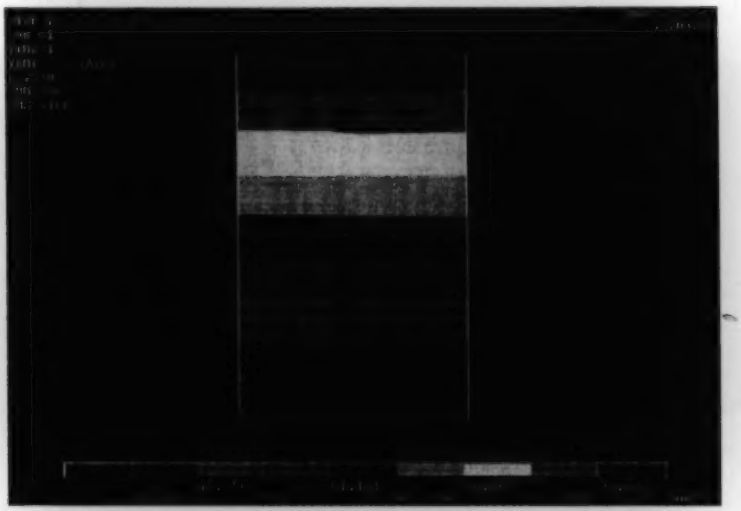

(a) Center cross-section view (width)

(b) Center cross-section view (length)

Figure 3.9: Temperature profile of the copper block under one-dimensional steady-state conduction heat transfer process obtained by a finite element analysis through ANSYS 7.0.

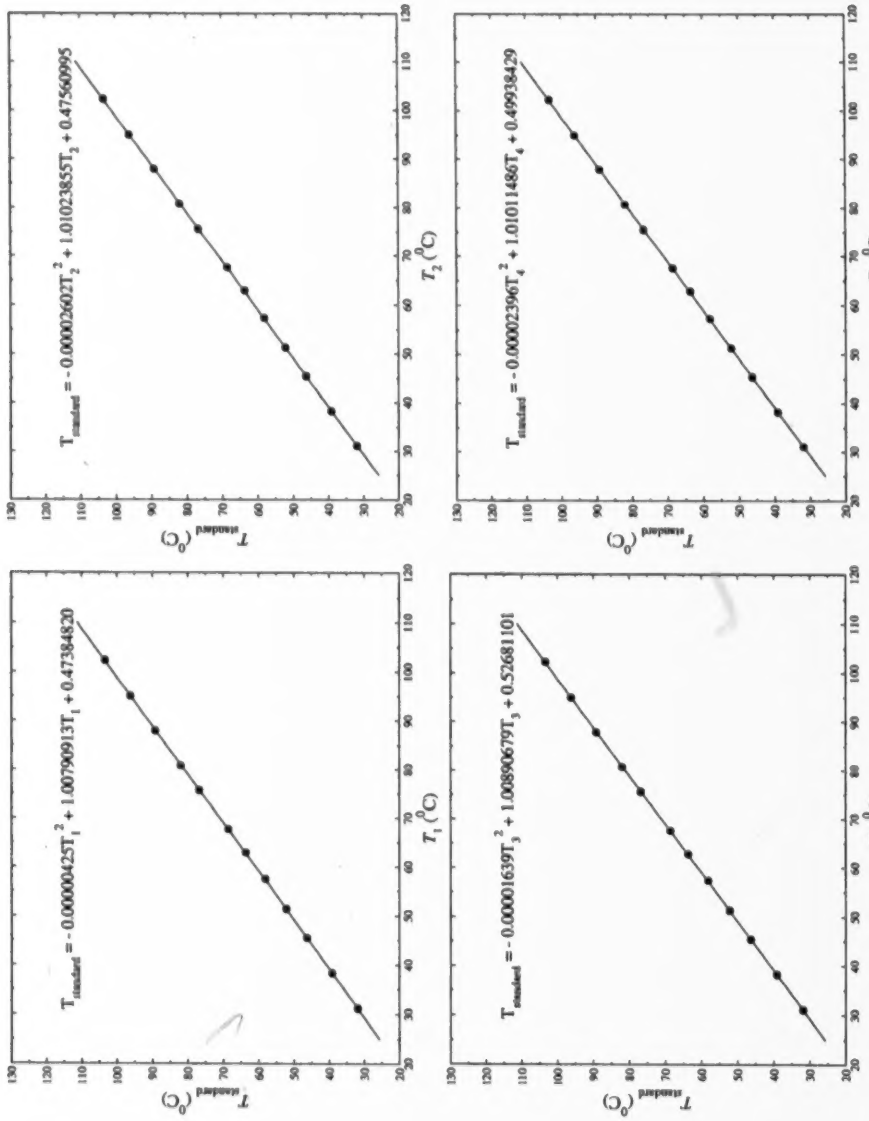

Figure 3.10: Polynomial regression curve-fittings of the four thermocouple probes.

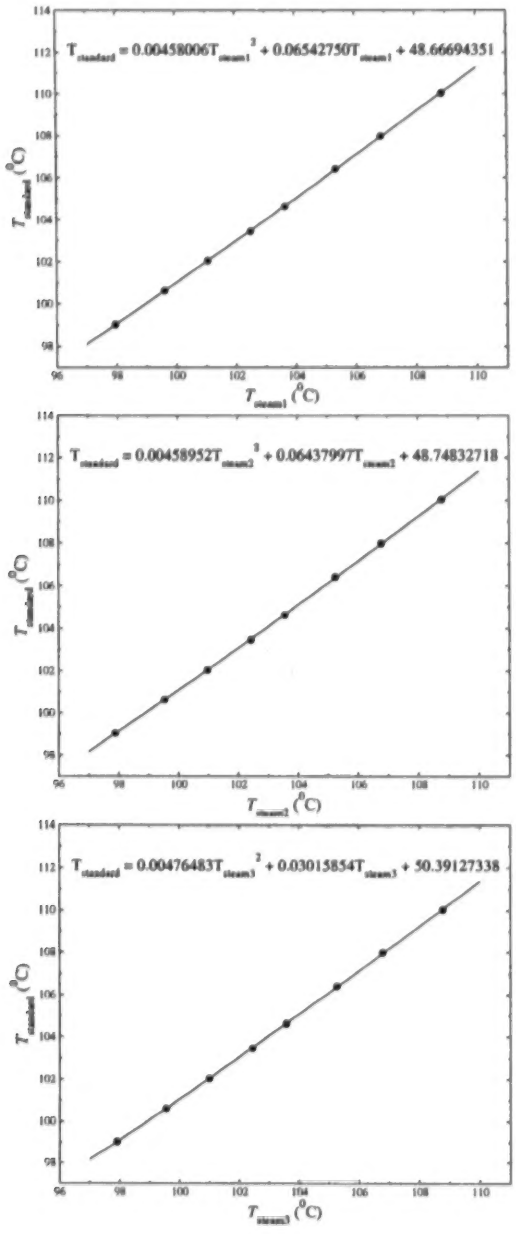

Figure 3.11: Polynomial regression curve-fittings of the three thermocouple wires.

Chapter 4

Results and Discussion

4.1 Application of SAMs at Same Heat Flux

4.1.1 Improvement of Heat Transfer Coefficient

Condensation experiments were first conducted on 16-mercaptohexadecanoic acid SAMs as it was expected that film condensation would occur. The experimental heat transfer coefficients h with time are displayed in Figure 4.1 for a heat flux q'' of $\sim$ 280 kW/m^2 and a subcooling temperature about ΔT of $\sim$ 43°C. The heat transfer coefficients calculated by the Nusselt theory for film condensation on a vertical plate [4, 64] according to the same condensation conditions are also given in the same figure. It can be seen that the experimental h for the 16-mercaptohexadecanoic acid is stable for more than 2 hours and agree with those predicted from the Nusselt theory, suggesting that the procedures and experimental setup for the determination of the heat transfer coefficient h is valid.

A series of DWC experiments were carried out by using 1-octadecanethiol SAMs as the promoter because of its hydrophobicity. For comparison, the steam velocity, condensation pressure and heat flux were maintained the same as that of the FWC

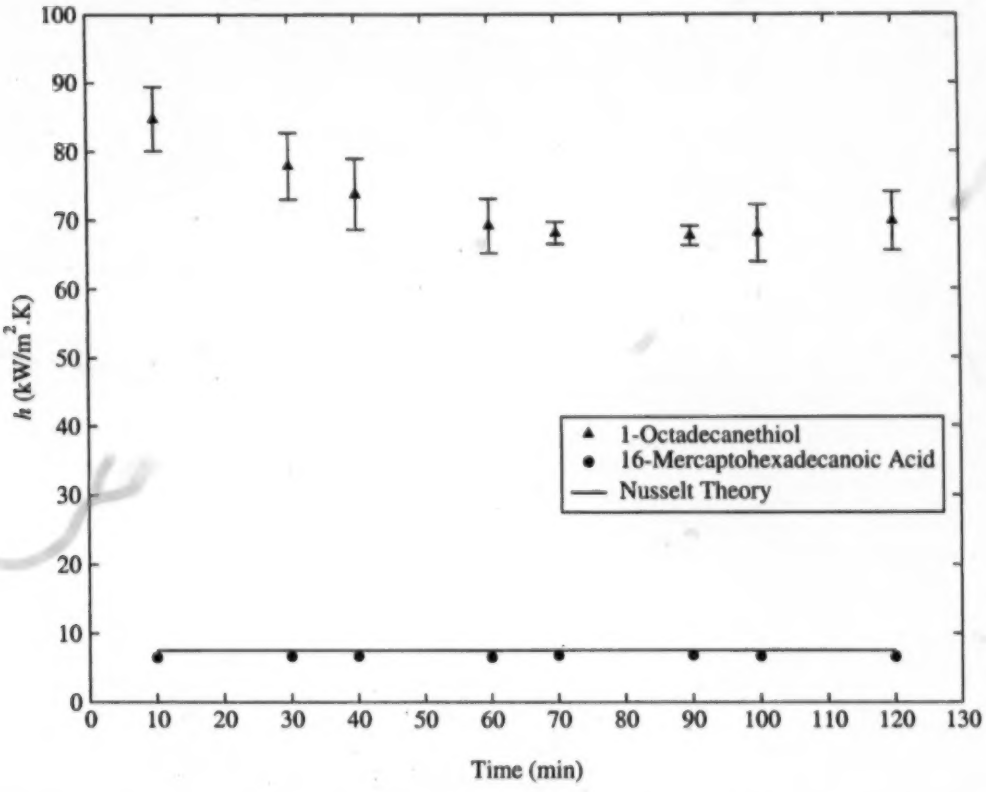

Figure 4.1: Condensation heat transfer coefficient of SAMs on evaporated Au/Ti/Cu substrates as a function of time during steam condensation at standard atmosphere pressure. Steam velocity passing through the condensing surface is $\sim$ 6 m/s and heat flux is $\sim$ 280 kW/m^2.

experiments. The experimental results over time for an average of 4 independent tests are also given in Figure 4.1. Figure 4.2 illustrates a picture of DWC of steam on the 1-octadecanethiol SAMs. As can be seen in Figure 4.1, the DWC heat transfer coefficient is in the order of 65 $\sim$ 85 kW/m^2·K, depending on the time of

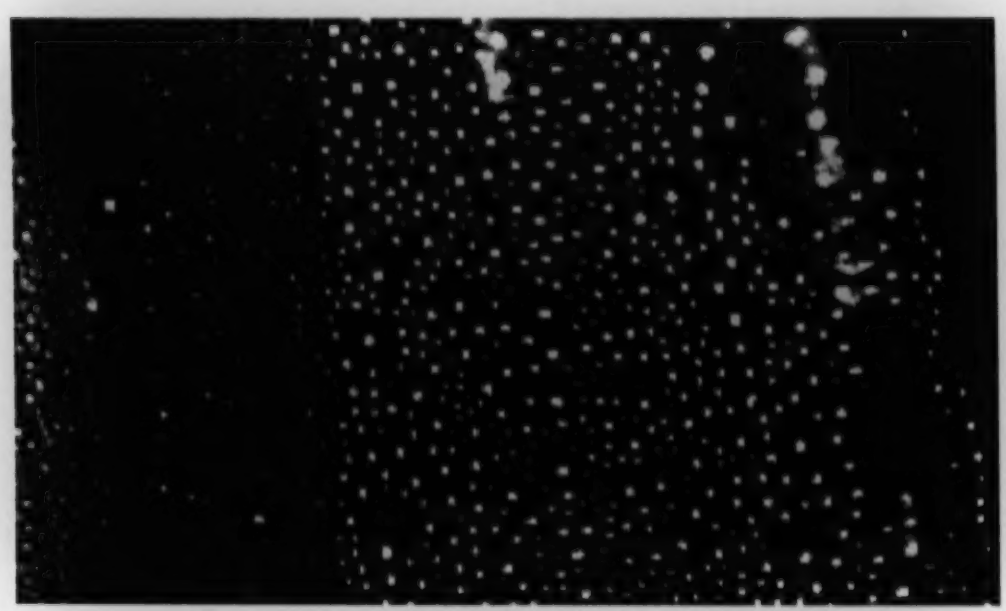

Figure 4.2: Dropwise condensation of steam on self-assembled monolayers (SAMs) derived from 1-octadecanethiol [$HS(CH_2)_{17}CH_3$] onto gold-coated-copper substrates.

experiments. This represents nearly an order of magnitude improvement over FWC and is similar to those reported by Das *et al.* [15, 16]. While Das *et al.* reported a constant h value for the $HS(CH_2)_{15}CH_3$ for each heat flux, the results presented here reveal that h is indeed time dependent for heat flux $\sim$ 280 kW/m^2; the heat transfer coefficient h starts at around 85 kW/m^2·K after 10 minutes of experiment and decreases to 65 kW/m^2·K after about one and half hour; eventually, it rises to 70 kW/m^2·K after about 2 hours. It should be pointed out that the error bars in Figure 4.1 are the 95% confidence limits, suggesting that the trends could be real. As SAMs are more stable the longer its chain length (up to about 22 carbons), it is

expected that the $HS(CH_2)_{15}CH_3$ SAMs used in [15, 16] would yield even a larger variation of h with time. This is different from the observations reported here. If the time dependent process of DWC on the $HS(CH_2)_{17}CH_3$ octadecanethiol is real, it was speculated that its surface properties would have changed over time. To elucidate this, an *ex situ* FT-IR and ellipsometry were used to monitor the changes in surface chemistry and film thickness, respectively.

4.1.2 Characterizations of SAMs

To relate the changed DWC heat transfer coefficient with the actual surface chemistry, an *ex situ* fourier transform infrared spectroscopy (FT-IR) and ellipsometry were used to characterize the SAMs during the condensation process. The octadecanethiol monolayers were first characterized by reflectance fourier transform infrared spectroscopy (FT-IR) and ellipsometry in terms of spectra and thickness, respectively, before the condensation experiment, i.e. at $t' = 0$. The copper block was then placed into the condenser for half an hour of condensation experiment before it was taken out for another surface characterization. These procedures were repeated every 30 minutes until an elapsed time of 2 hours have reached. Figure 4.3 displays the reflectance infrared spectra for SAMs derived from 1-octadecanethiol on Au/Ti/Cu substrates subjected to the steam condensation process at various duration for $q'' \approx 280$ kW/m^2. Figures 4.4 and 4.5 show, respectively, the normalized thickness and heat transfer coefficient as a function of condensation duration for $q'' \approx 280$ kW/m^2.

In Figure 4.3 for $t' = 0$, the asymmetric methylene peaks $\nu_a(CH_2)$ appeared at

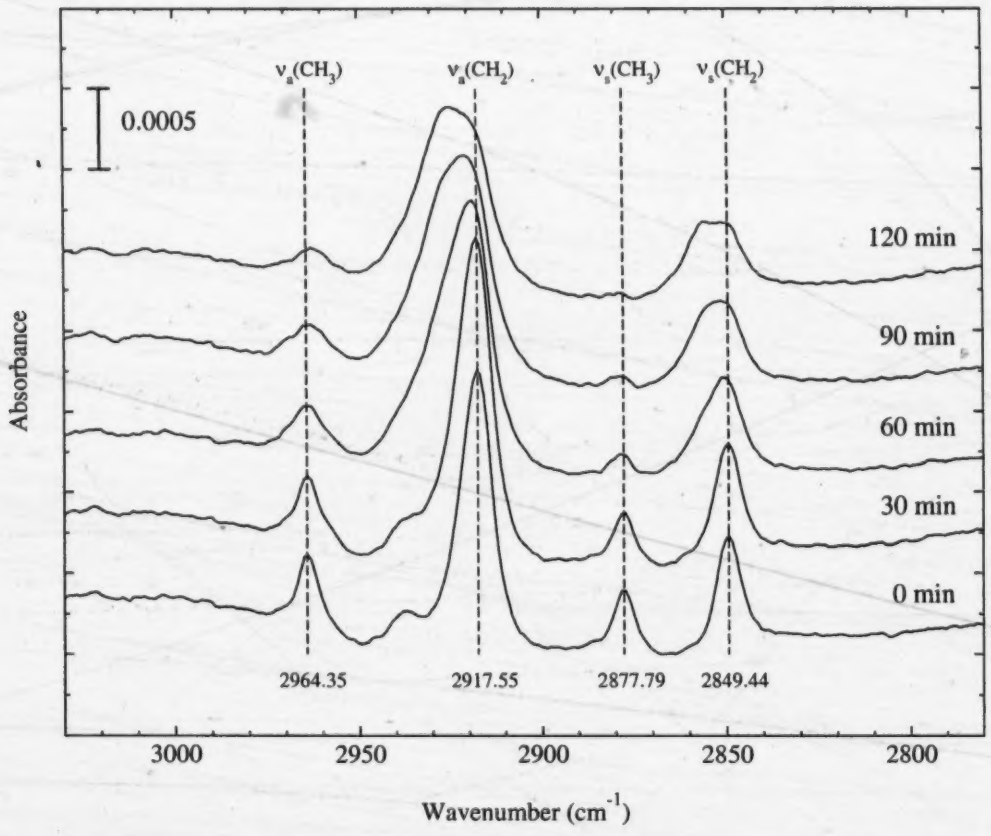

Figure 4.3: Reflectance FT-IR spectra for SAMs derived from 1-octadecanethiol on Au/Ti/Cu substrates subjected to steam condensation in various duration ($q'' \approx$ 280 kW/m^2). The dashed lines represent the positions of the original modes for a trans-extended monolayer. The spectra have been offset for clarity.

~ 2918 cm^{-1}, indicating a primarily trans-zigzag extended hydrocarbon chain with few gauche conformers. The spectra demonstrate that SAMs of 1-octadecanethiol adsorbed onto Au are highly crystalline. This is independently confirmed by the ellipsometry results giving the initial thickness as 2.36 nm at $t' = 0$, in agreement

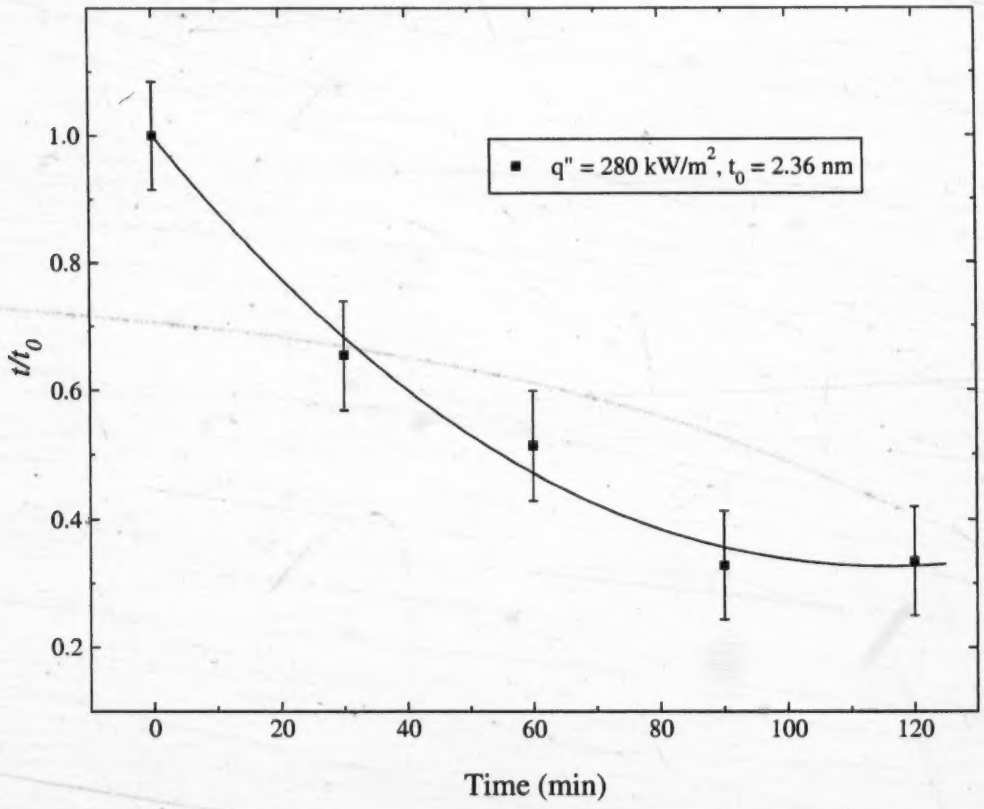

Figure 4.4: Normalized thickness of SAMs derived from 1-octadecanethiol on gold-coated-copper substrates as a function of condensation duration for heat flux $q'' \approx 280$ kW/m^2. t_0 is the initial film thickness reference. Error bars are $\pm$ 0.2 nm in reference to t_0 and represent typical measurement errors for ellipsometry.

with the theoretical thickness of 2.2 nm [65] and those reported in the literature [66, 36] for a closely packed octadecanethiol adsorbed onto gold. For $t' > 0$, however, it can be seen in Figure 4.3 that nearly all spectra intensities decrease with the time of condensation, suggesting lost of monolayer with time. For trans-zigzig and

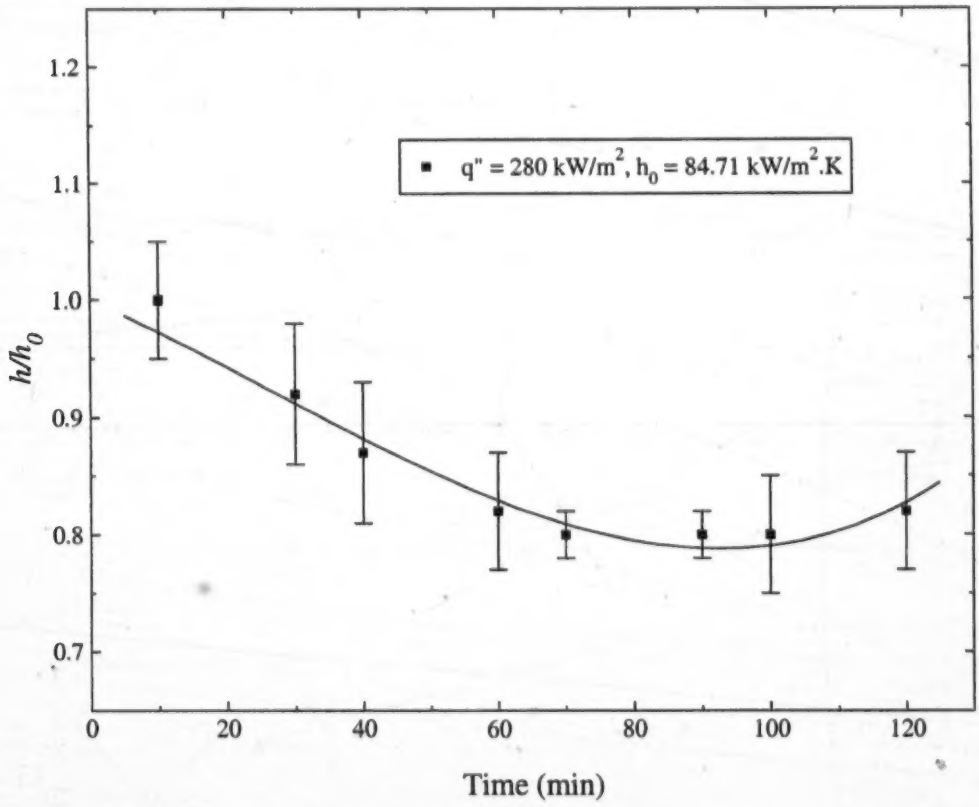

Figure 4.5: Normalized heat transfer coefficient as a function of condensation duration for heat flux $q'' \approx 280$ kW/m^2. h_0 is the heat transfer coefficient after 10 minute condensation. Error bars are 95% confidence limits.

highly-ordered conformations, the methylene asymmetric $\nu_a(CH_2)$ and symmetric $\nu_s(CH_2)$ modes should be below 2918 cm^{-1} and 2850 cm^{-1}, respectively [66, 36]. Deviation of the methylene peak positions from these values for $t' > 0$ reflects that these monolayers have become less crystalline [67, 68, 69]. During condensation process, the intensity of the asymmetric and symmetric methylene ($\nu_a(CH_2)$ and

$\nu_s(CH_2)$) stretching mode increases slightly after 30 minutes and began to decrease continuously with time; while intensities for $\nu_a(CH_3)$ and $\nu_a(CH_3)$ decrease with time. Also note that the spectra exhibit peak broadening for all C-H stretching modes with time. These results indicate that the 1-octadecanethiol SAMs are still crystalline at $t' = 30$ minutes; while some monolayers have already been peeled off after 30 minutes. Thus, the tilt angle of the alkyl chain increases from the surface normal, exposing more methylene groups to the surface and resulting in the initial increase in $\nu_a(CH_2)$. After 90 minutes, the intensity of $\nu_s(CH_3)$ is nearly zero, suggesting that the monolayers are loosely packed and the infrared hardly sees any methyl groups as they are blocked by the flexible methylene backbone. This interpretation is confirmed by the independent ellipsometry results in Figure 4.4 that the normalized film thickness decreases with time and reaches a plateau after $t' = 90$ minutes. Here, the condenser surface appears to have patches of the bare metals without the monolayers and should result in a mixture of dropwise and filmwise condensation. The lost in SAMs indicated from the above FT-IR and ellipsometry results are in good agreement with the general behavior of the experimental heat transfer coefficient h with time as shown in Figure 4.5. It can be seen that as SAMs become less crystalline (decrease in thickness), the heat transfer coefficient decreases gradually during the first 90 minutes condensation process.

A very interesting phenomenon, however, occurs in Figure 4.5. As SAMs are being removed after $t' = 90$ minutes, one would expect a mixture of filmwise and dropwise condensation to coexist, which should reduce the total effective heat transfer coefficient. This expectation is not met in Figure 4.5: h, however, increases

slightly with time after $t' = 90$ minutes. The reason for this phenomena is not clear and requires further study. Presumably, when SAMs are removed exposing patches of the bare metal, contamination from steam would quickly adsorb on such high energy sites, causing localized DWC and results in a slightly higher effective heat transfer coefficient [2, 3, 4, 5, 6]. This is partly confirmed from the results in Figure 4.4 that the film thickness increases slightly after $t' = 90$ minutes.

The conclusions obtained here would not have been possible without the use of infrared spectroscopy and ellipsometry. It is concluded that surface properties are important factors in dropwise condensation. Understanding this process through surface modifications of organic monolayers requires careful experimentation and analytical tools.

4.2 Application of SAMs at Different Heat fluxes

To verify the results in the previous section that were obtained at a single heat flux, a series of film and dropwise condensation experiments at different heat fluxes were carried out using the same 1-octadecanethiol and 16-mercaptohexadecanoic acid SAMs on Au/Ti/Cu substrates. For the sake of comparison, the condensation pressure was set to be standard atmosphere pressure and the steam velocity was controlled to be $\sim$ 6 m/s, the same as before.

4.2.1 Film Condensation

For film condensation, heat fluxes q'' of $\sim$ 140, 200, 230 and 270 kW/m^2 were selected. It is should be pointed out that, for film condensation, 280 kW/m^2 is nearly the largest heat flux that can be obtained by using the domestic water from the building as coolant for this experimental set-up, as described in section 3.3.3. The 16-mercaptohexadecanoic acid SAMs on Au/Ti/Cu substrate were inserted into the condensing chamber for 2 hours and the heat transfer coefficients were measured every 10 or 20 minutes.

The results are shown in Figure 4.6 together with those heat transfer coefficients calculated by the Nusselt theory for film condensation on a vertical plate [4, 64]. It can be seen that, for all heat fluxes, the heat transfer coefficients are in the order of 8$\sim$10 kW/m^2·K, in good agreement with those in the literature for film condensation of steam [70, 71, 72]. For the first half an hour, the heat transfer coefficients increase slightly and then become stable for the next one and half hours. This means that, when exposed to steam, the surface energy of 16-

mercaptohexadecanoic acid SAMs decreases slightly at the beginning and then stabilizes for a while. Therefore, 16-mercaptohexadecanoic acid SAMs are very effective to protect high surface energy gold surface from contamination via steam for more than 2 hours. Figure 4.6 also shows that, the experimental heat transfer coefficients agree well with those predicted from the Nusselt theory for each heat flux, suggesting that our procedures and experimental set-up for the determination of heat transfer coefficient is valid.

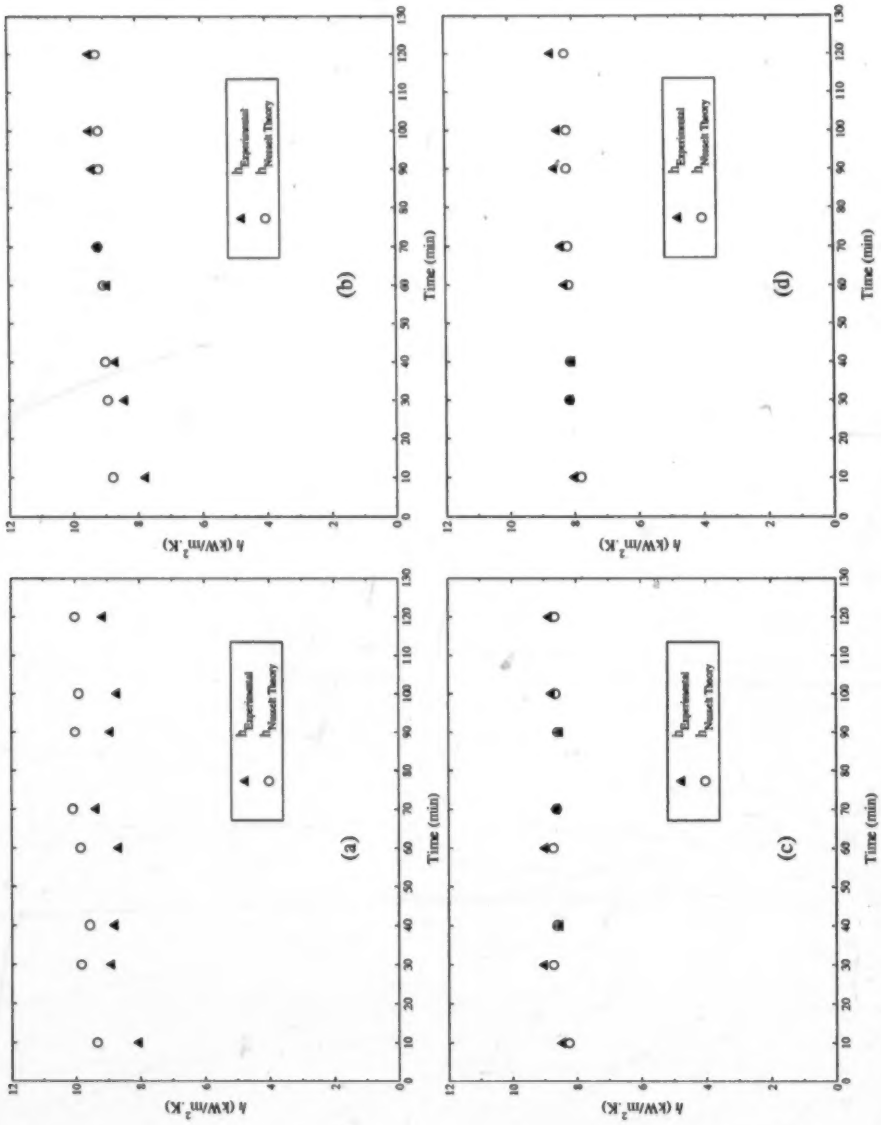

Figure 4.6: Experimental and theoretical film condensation heat transfer coefficients of 16-mercaptohexadecanoic acid SAMs on evaporated Au/Ti/Cu substrates as a function of time during steam condensation: (a) $q'' \approx 140$ kW/m^2; (b) $q'' \approx 200$ kW/m^2; (c) $q'' \approx 230$ kW/m^2; (d) $q'' \approx 270$ kW/m^2.

4.2.2 Dropwise Condensation

4.2.2.1 Measurement of Heat Transfer Coefficient

According to the cooling capacity of domestic water from the building, four other heat fluxes q'' of $\sim$ 320, 360, 400 and 460 kW/m^2 were chosen for DWC experiments. The reason for this is that, for heat fluxes over 460 kW/m^2 and less than 280 kW/m^2, it is very difficult to obtain stable measurements of heat transfer coefficient because of the lack of stable coolant water flow. For each heat flux, 4 independent tests were conducted. The reported heat transfer coefficient is the average of the four tests. The experimental process is the same as that described in section 4.1.2: The 1-octadecanethiol SAMs were first characterized by reflectance fourier transform infrared spectroscopy (FT-IR) and ellipsometry in terms of spectra and thickness, respectively, before the condensation experiment, i.e. at $t' = 0$. The copper block was then placed into the condenser for half an hour and heat transfer coefficients were measured before it was taken out for another surface characterization. These procedures were repeated every 30 minutes until an elapsed time of 2 hours has reached.

Figures 4.7, 4.8, 4.9 and 4.10 show, respectively, the heat transfer coefficient as a function of condensation duration for heat fluxes of $\sim$ 320, 360, 400 and 460 kW/m^2. It can be seen that, as same as the results of heat flux of $\sim$ 280 kW/m^2 (Figure 4.1), the DWC heat transfer coefficients for all heat fluxes are in the order of 70 $\sim$ 90 kW/m^2·K, depending on the time of experiments. While Das *et al.* [15, 16] reported a constant h value for the $HS(CH_2)_{15}CH_3$ SAMs for each heat flux, these results reveal that h is indeed time dependent for all heat fluxes: the

heat transfer coefficient starts at $\sim$ 90 kW/m^2·K after 10 minutes of experiment, decreases to $\sim$ 70 kW/m^2·K after a while and eventually rises to $\sim$ 80 kW/m^2·K after 2 hours. The difference between each heat flux is:

1. For heat flux q'' of $\sim$ 280 kW/m^2, the heat transfer coefficient h decreases to the lowest point around 90 minutes after start and rises to $\sim$ 70 kW/m^2·K (see Figure 4.1) after 2 hours;

2. For heat flux q'' of $\sim$ 320 kW/m^2, h decreases to the lowest point around 70 minutes and rises to $\sim$ 81 kW/m^2·K (see Figure 4.7);

3. The trend of h for heat flux q'' of $\sim$ 360 kW/m^2 is similar to that for q'' of $\sim$ 320 kW/m^2 (see Figure 4.8);

4. For heat fluxes q'' of $\sim$ 400 and 460 kW/m^2, h decreases to the lowest point around 60 and 30 minutes and rise to 81 and 83 kW/m^2·K, respectively (see Figures 4.9 and 4.10).

The results of heat transfer coefficients for different heat fluxes not only further verify that DWC on 1-octadecanethiol SAMs is a time dependent process, but also indicate that surface properties of 1-octadecanethiol SAMs on Au/Ti/Cu substrates would have changed with heat flux passing through the surface. To elucidate this, an *ex situ* FT-IR and ellipsometry were used to monitor the changes in surface chemistry and film thickness, respectively.

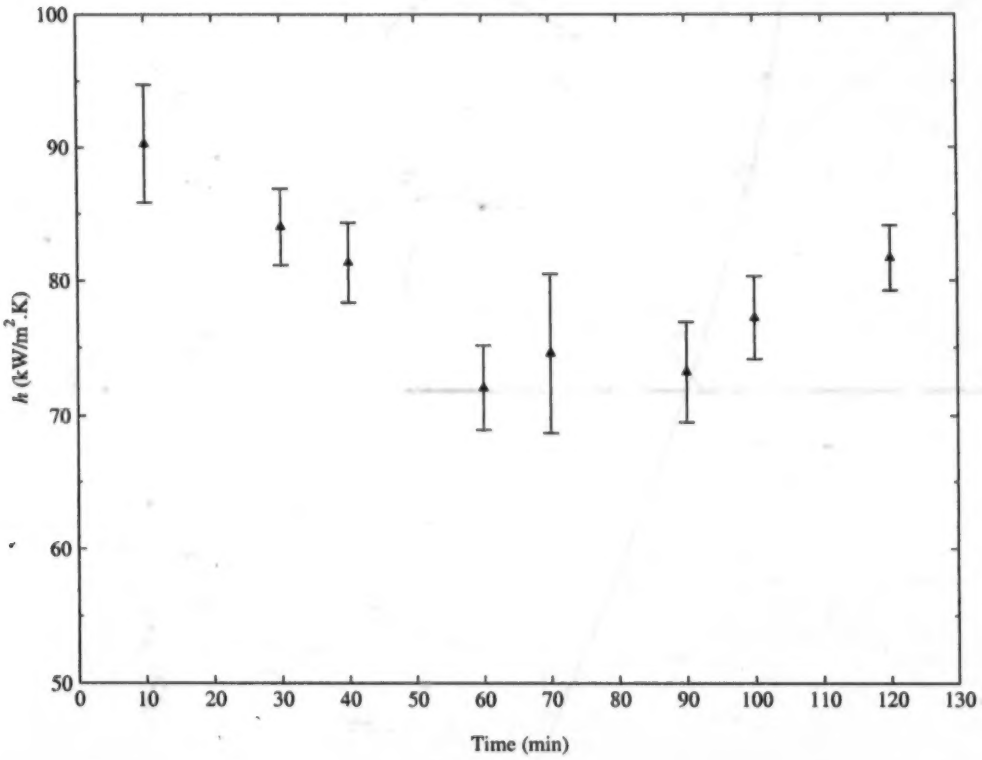

Figure 4.7: Heat transfer coefficient as a function of condensation duration for heat flux $q'' \approx 320$ kW/m^2. Error bars are 95% confidence limits.

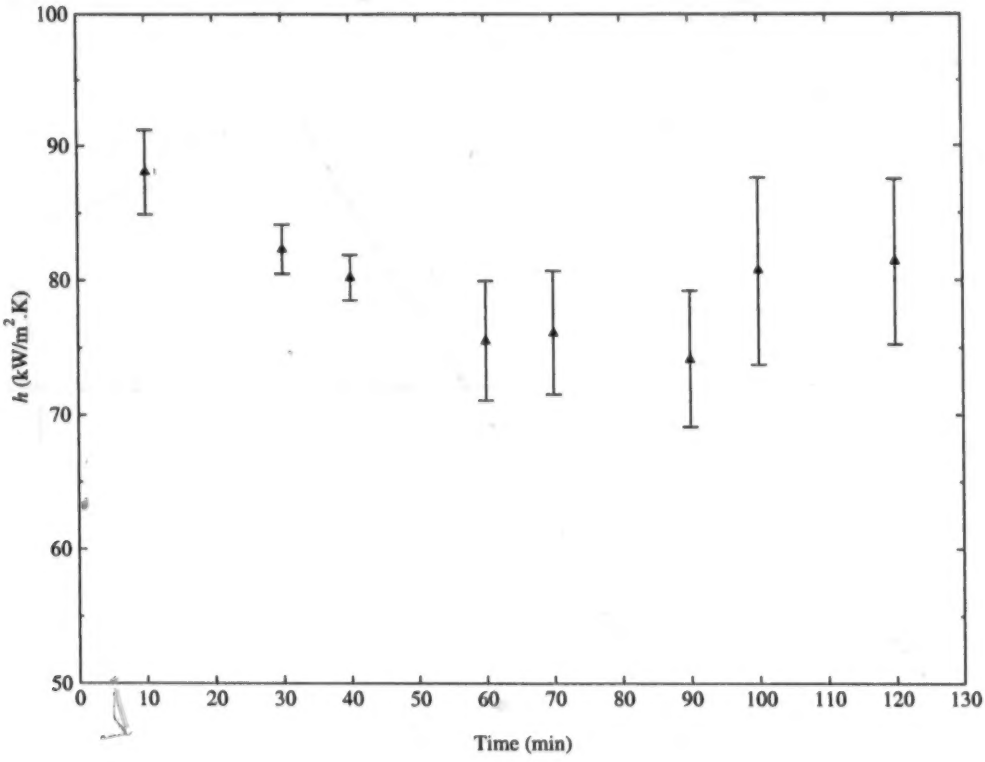

Figure 4.8: Heat transfer coefficient as a function of condensation duration for heat flux $q'' \approx 360$ kW/m^2. Error bars are 95% confidence limits.

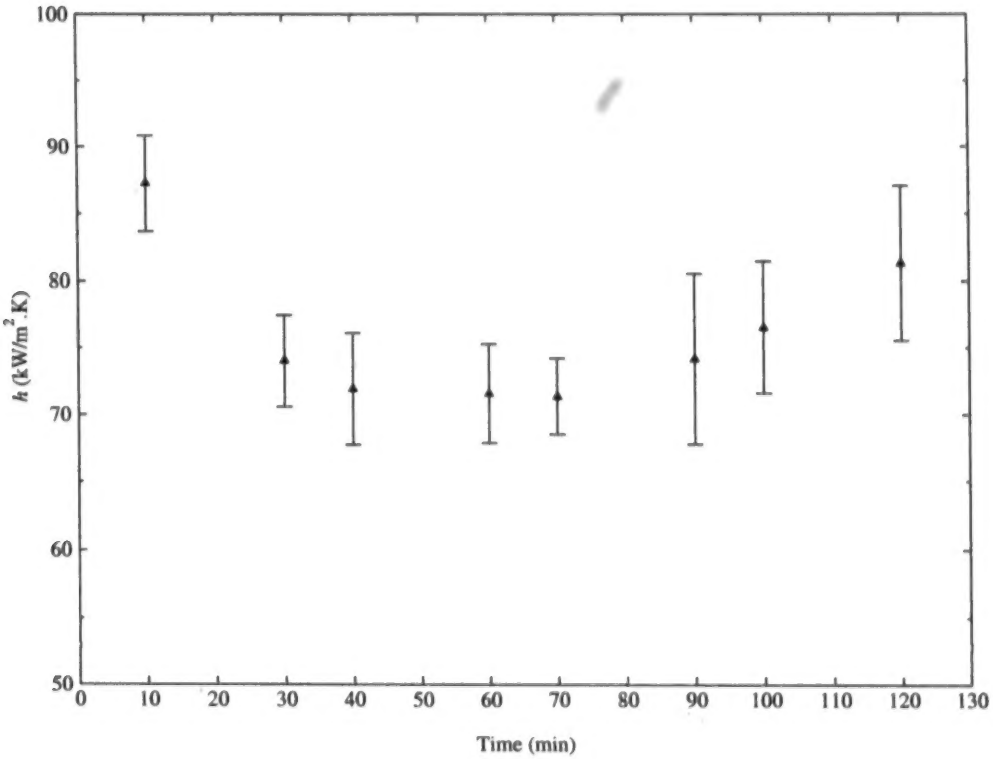

Figure 4.9: Heat transfer coefficient as a function of condensation duration for heat flux $q'' \approx 400$ kW/m^2. Error bars are 95% confidence limits.

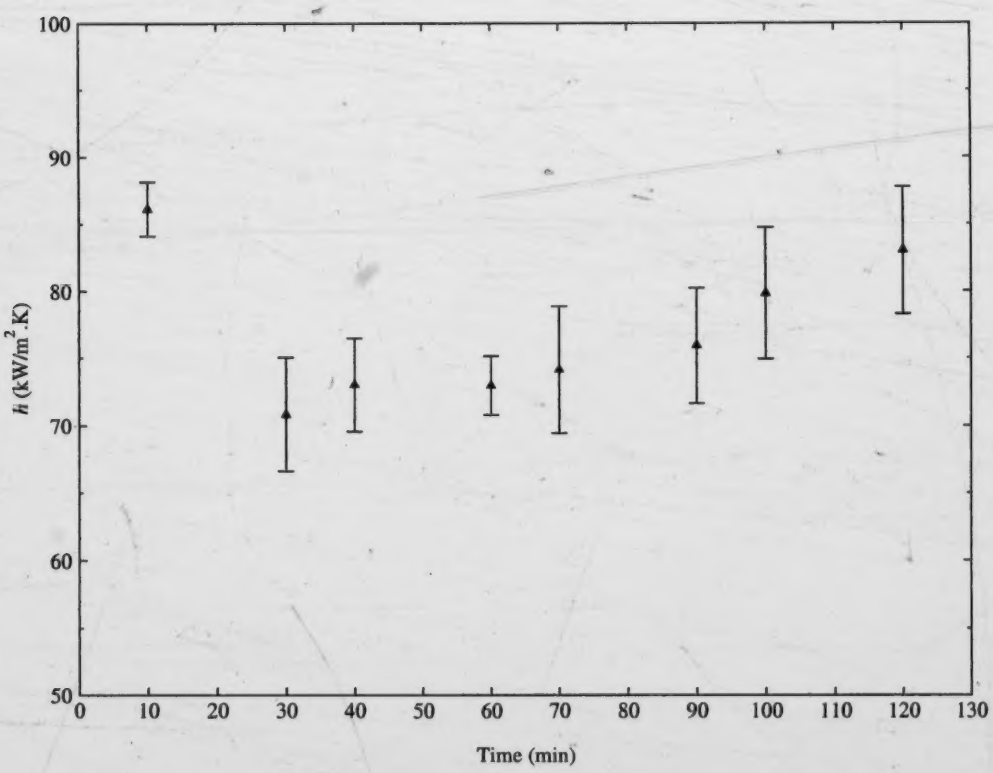

Figure 4.10: Heat transfer coefficient as a function of condensation duration for heat flux $q'' \approx 460$ kW/m^2. Error bars are 95% confidence limits.

4.2.2.2 Characterizations of SAMs

To relate the changed DWC heat transfer coefficient with the actual surface chemistry, an *ex situ* fourier transform infrared spectroscopy (FT-IR) and ellipsometry were used to characterize the SAMs during the condensation process. Figures 4.11, 4.12, 4.13 and 4.14 display, respectively, the reflectance infrared spectra for SAMs derived from 1-octadecanethiol on Au/Ti/Cu substrates subjected to the steam condensation process at various duration for heat fluxes of $\sim$ 320, 360, 400 and 460 kW/m^2. Figures 4.15 and 4.16 show, separately, the normalized thickness and heat transfer coefficient as a function of condensation duration for all heat fluxes (for the sake of comparison, the normalized thickness and heat transfer coefficient for heat flux of $\sim$ 280 kW/m^2 are also shown in these two figures). It should be pointed out that, for Figure 4.15, error bars of each point are $\pm$ 0.2 nm in reference to t_0 and represent typical measurement errors for the particular ellipsometry used. For clarity, they are not shown. For Figure 4.16, measurement errors can be seen in Figures 4.1, 4.7, 4.8, 4.9 and 4.10.

In Figures 4.11, 4.12, 4.13 and 4.14, for $t' = 0$, the asymmetric and symmetric methylene peaks ($\nu_a(CH_2)$ and $\nu_s(CH_2)$) appeared at $\sim$2918 cm^{-1} and 2850 cm^{-1}, respectively; the asymmetric and symmetric methyl peaks ($\nu_a(CH_3)$ and $\nu_s(CH_3)$) appeared at $\sim$ 2965 cm^{-1} and 2878 cm^{-1}, separately. These spectra demonstrate that all the SAMs formed were highly crystalline [67, 68, 69]. This is independently comfirmed by the ellipsometry results which show that the initial thickness for the four heat fluxes are 2.23, 2.52, 2.18 and 2.42 nm (Figure 4.15), in good agreement with the theoretical thickness of 2.2 nm [65] and those reported in the literature

[66, 36] for a closely packed 1-octadecanethiol adsorbed onto gold.

For $t' > 0$, it can be seen from Figures 4.11, 4.12, 4.13 and 4.14 that, for each heat flux, the results are the same as those for a heat flux of ~ 280 kW/m^2 (Figure 4.3): nearly all spectra exhibit decreasing intensities and peak broadening with the increasing time of condensation, suggesting that SAMs have become less crystalline during the condensation process [67, 68, 69]. The difference between them is: for a heat flux of ~ 280 kW/m^2, the intensity of the asymmetric and symmetric methylene stretching modes ($\nu_a(CH_2)$ and $\nu_s(CH_2)$) increases slightly for 30 minutes and decreases continuously thereafter; but for heat fluxes of $\sim$ 320, 360, 400 and 460 kW/m^2, only the intensity of the asymmetric methylene ($\nu_a(CH_2)$) stretching mode increases slightly for the first 30 minutes, while all intensities for $\nu_s(CH_2)$, $\nu_a(CH_3)$ and $\nu_s(CH_3)$ decrease continuously with time; the spectra changes for heat fluxes of $\sim$ 320, 360 and 400 kW/m^2 are very similar, except that, at $t' = 60$ and 90 minutes, the intensities of $\nu_s(CH_3)$ and $\nu_a(CH_3)$ for $q'' \approx 400$ kW/m^2 are less than that for $q'' \approx 320$ and 360 kW/m^2; for a heat flux of ~ 460 kW/m^2, the changes of spectra with condensation duration become more serious: at $t' = 60$ minutes, the intensities of $\nu_s(CH_3)$ and $\nu_a(CH_3)$ almost become negligible; at $t' = 120$ minutes, even the intensities of $\nu_s(CH_2)$ and $\nu_a(CH_2)$ are nearly zero.

These FT-IR spectroscopy results indicate that the 1-octadecanethiol SAMs are still crystalline at $t' = 30$ minutes for all heat fluxes; while some monolayers begin to peel off after 30 minutes, exposing more methylene groups to the surface. After $t' > 30$ minutes, more and more monolayers peel off from the surface, suggesting

that the SAMs become loosely packed and result in the decrease in intensity of the methyl and methylene stretching modes; the rate that monolayers peel off from the surface depends on the heat flux passing through the surface: the more the heat flux, the faster monolayers peel off from the surface.

The interpretation of FT-IR spectra is comfirmed by the independent ellipsometry results as shown in Figure 4.15: the normalized film thickness decreases with time for each heat flux; while for different heat fluxes, the rates that the film thickness decreases are different: the larger the heat flux, the faster the film thickness decreases.

The lost of SAMs with time and the heat flux dependent SAMs' removal indicated from the above FT-IR and ellipsometry results are in good agreement with the general behavior of the experimental heat transfer coefficient h with time for different heat fluxes as shown in Figure 4.16: as SAMs become less crystalline (decrease in thickness), the heat transfer coefficient decreases gradually with condensation duration; the more the heat flux, the faster the heat transfer coefficient reaches a plateau.

Furthermore, similar to the results for a heat flux of ~ 280 kW/m^2, the phenomenon that heat transfer coefficient increases after decreasing to a plateau occurs for all other heat fluxes in Figure 4.16. The heat transfer coefficient that could reach after 2 hours condensation duration also increases when heat flux increases. This phenomenon is also confirmed from the ellipsometry results in Figure 4.15 that the film thickness increases slightly after it reaches a plateau for each heat flux. The reason for this phenomenon is unclear and requires further study. Presum-

ably, when SAMs are removed exposing patches of the bare gold, contamination from steam would quickly adsorb on such high energy sites, causing localized DWC and resulting in a slightly higher effective heat transfer coefficient [2, 3, 4, 5, 6]; the more the heat flux, the faster exposing patches of the bare gold and the more contamination adsorbed onto the bare gold surface.

Therefore, caution should be taken when applying SAMs as DWC promoters. The conclusions obtained here would not have been possible without the use of infrared spectroscopy and ellipsometry to characterize the surface properties in dropwise condensation.

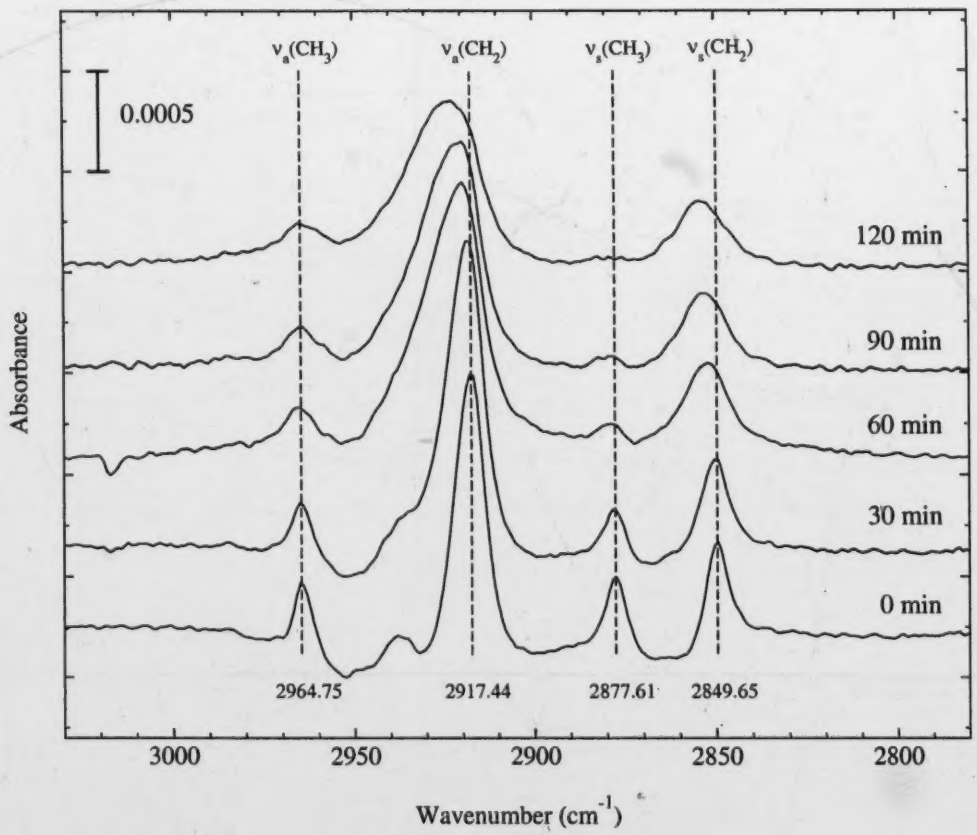

Figure 4.11: Reflectance FT-IR spectra for SAMs derived from 1-octadecanethiol on Au/Ti/Cu substrates subjected to steam condensation in various duration ($q'' \approx$ 320 kW/m^2). The dashed lines represent the positions of the original modes for a trans-extended monolayer. The spectra have been offset for clarity.

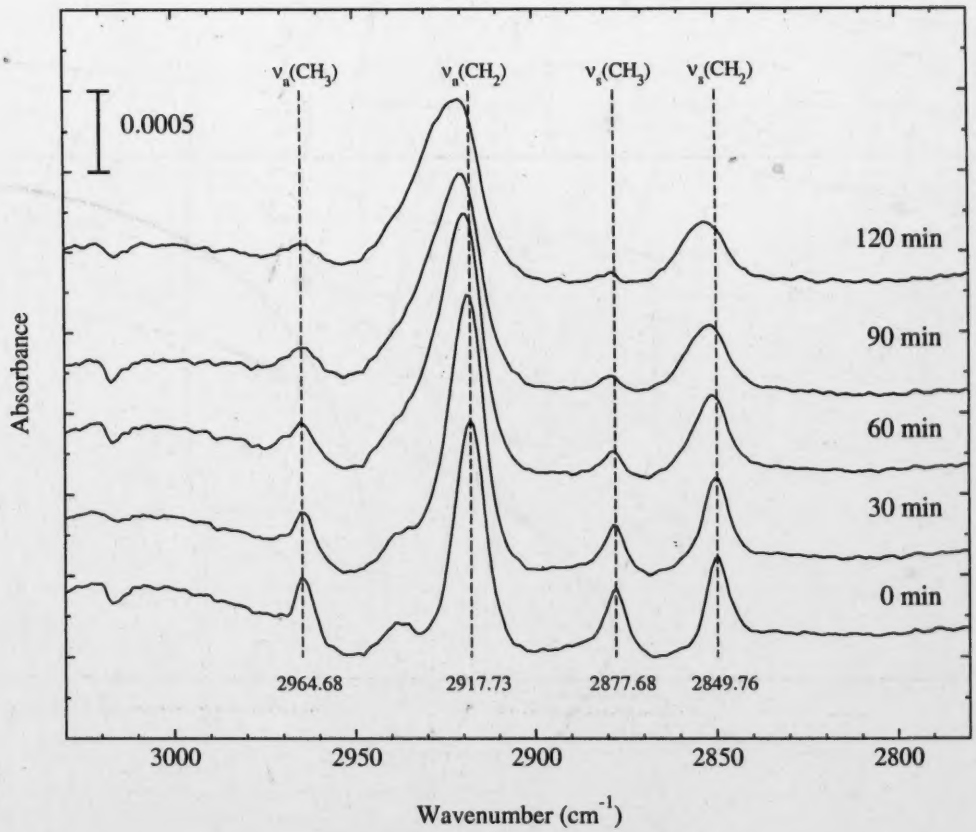

Figure 4.12: Reflectance FT-IR spectra for SAMs derived from 1-octadecanethiol on Au/Ti/Cu substrates subjected to steam condensation in various duration ($q'' \approx$ 360 kW/m^2). The dashed lines represent the positions of the original modes for a trans-extended monolayer. The spectra have been offset for clarity.

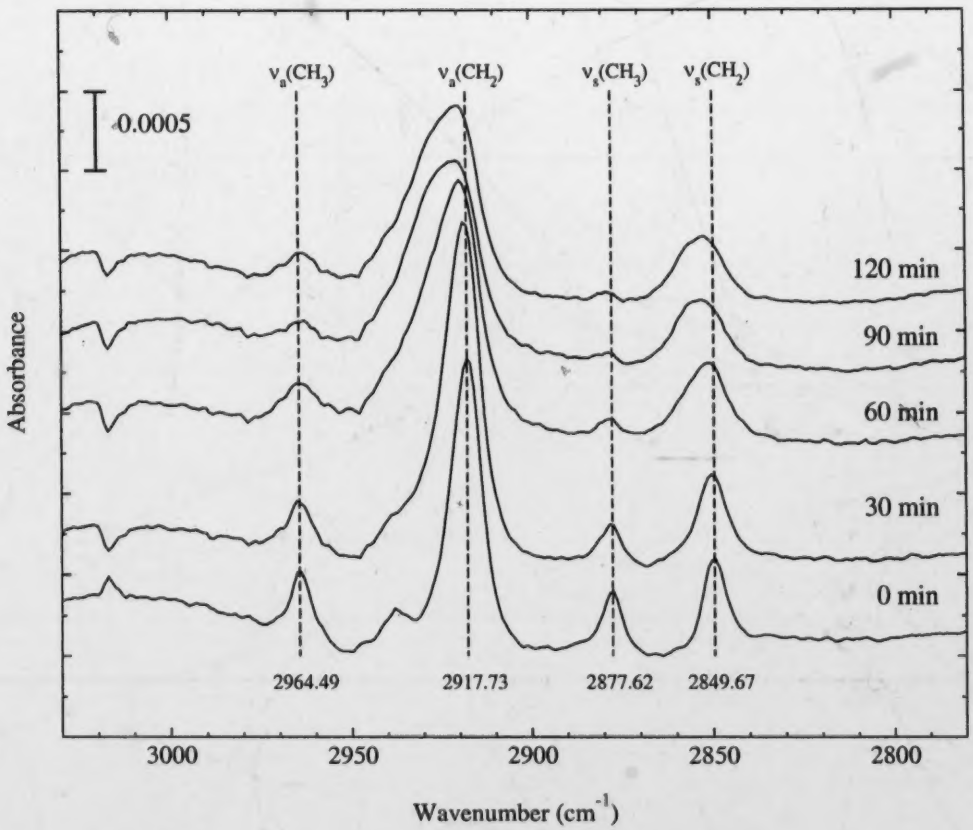

Figure 4.13: Reflectance FT-IR spectra for SAMs derived from 1-octadecanethiol on Au/Ti/Cu substrates subjected to steam condensation in various duration ($q'' \approx$ 400 kW/m^2). The dashed lines represent the positions of the original modes for a trans-extended monolayer. The spectra have been offset for clarity.

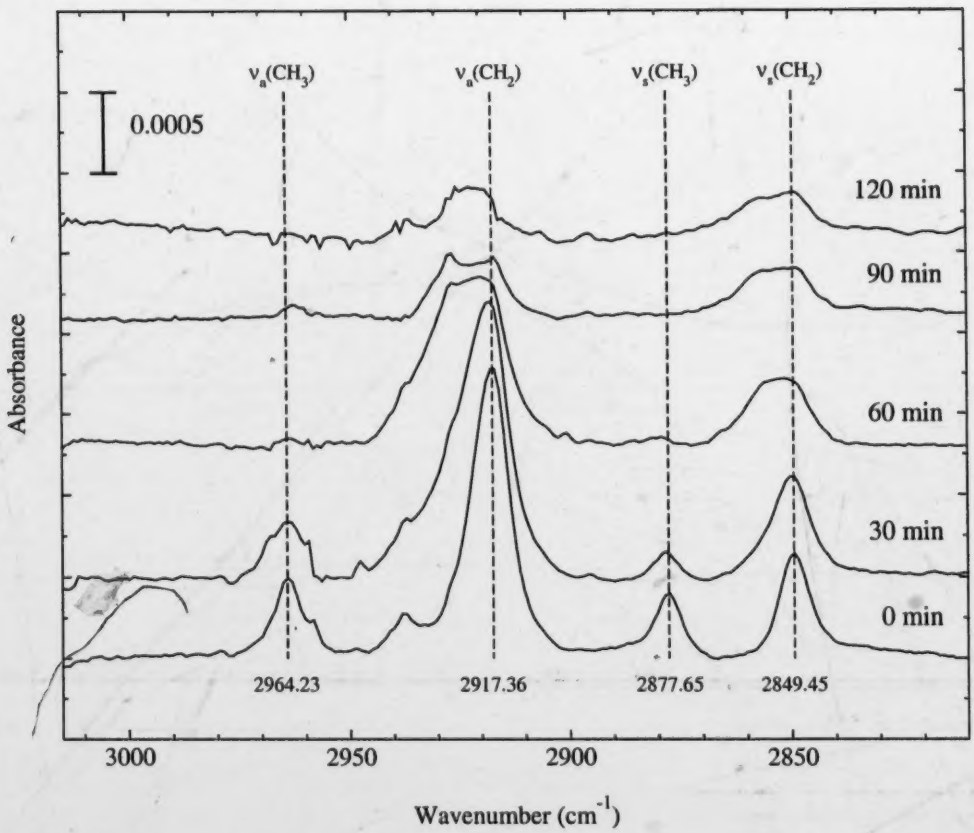

Figure 4.14: Reflectance FT-IR spectra for SAMs derived from 1-octadecanethiol on Au/Ti/Cu substrates subjected to steam condensation in various duration ($q'' \approx$ 460 kW/m^2). The dashed lines represent the positions of the original modes for a trans-extended monolayer. The spectra have been offset for clarity.

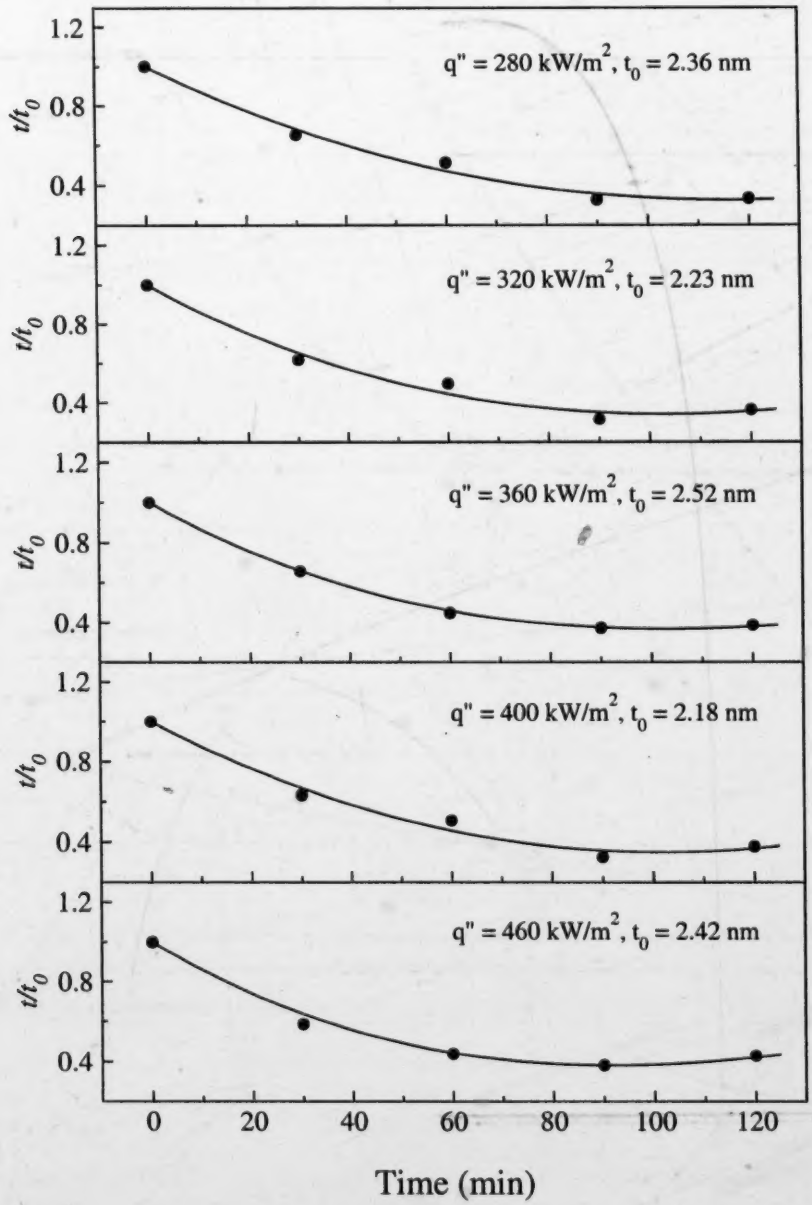

Figure 4.15: Normalized thickness of SAMs derived from 1-octadecanethiol on Au/Ti/Cu substrates as a function of condensation duration for different heat fluxes. t_0 is the initial film thickness reference.

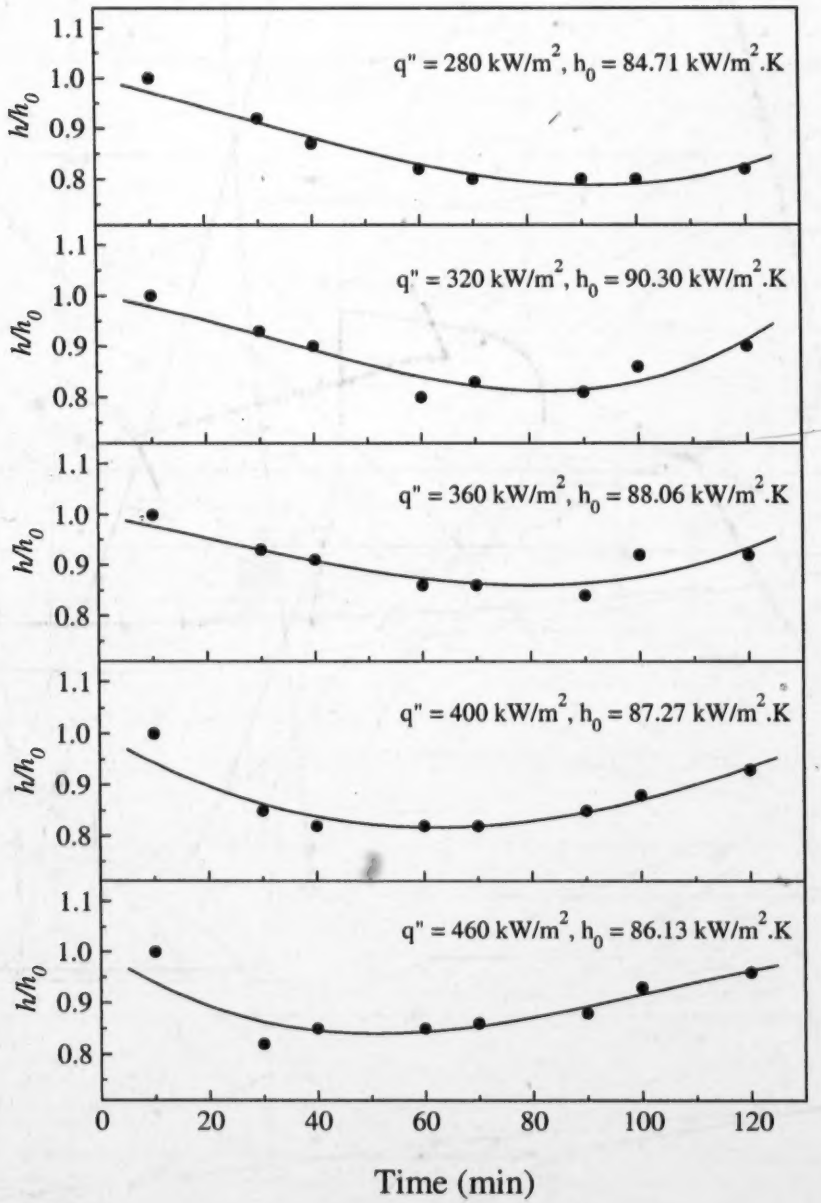

Figure 4.16: Normalized heat transfer coefficient of SAMs derived from 1-octadecanethiol on Au/Ti/Cu substrates as a function of condensation duration for different heat fluxes. h_0 is the heat transfer coefficient after 10 minute condensation.

Chapter 5

Conclusions and Future Research

5.1 Conclusions

An integrated study of dropwise condensation (DWC) heat transfer of steam using self-assembled monolayers (SAMs) adsorbed onto thermal evaporated Au/Ti/Cu substrates by means of fourier-transform infrared spectroscopy (FT-IR) and spectroscopic ellipsometry has been performed in this research. Both 1-octadecanethiol and 16-mercaptohexadecanoic acid SAMs were employed as the coatings for dropwise and film condensation, respectively, on a vertical surface. It was found that film condensation results for the 16-mercaptohexadecanoic acid SAMs are in good agreement with those from the Nusselt theory. When the 1-octadecanethiol SAMs was employed as a promoter, the heat transfer coefficient increased by nearly an order of magnitude due to dropwise condensation. It was also found that dropwise condensation on the 1-octadecanethiol SAMs is a dynamic process, producing a heat transfer coefficient that was time and heat flux dependent. These results were reconfirmed, for the first time, through fourier transform infrared spectroscopy (FT-IR) and spectroscopic ellipsometry studies.

Based on the experimental results, the following conclusions can be drawn:

1. In general, decreases in SAMs' crystallinity and film thickness over condensation duration cause the heat transfer coefficient to decrease, but not monotonically;

2. The larger the heat flux, the faster SAMs become less crystalline (decrease in thickness), resulting in a faster decrease of heat transfer coefficient with increasing heat flux;

3. Partial removal of SAMs exposes the bare gold to the steam. Spontaneous adsorption of contamination onto these high energy patches appears to cause the heat transfer coefficient to increase.

4. The thermal stability of self-assembled monolayers derived from adsorption of 16-mercaptohexadecanoic acid and 1-octadecanethiol onto gold substrates when exposed to steam are different.

5. Understanding of surface effects on the heat transfer coefficient would not have been possible without the use of a spectroscopic ellipsometry and FT-IR spectroscopy.

5.2 Future Work

In order to expand the systematic study of dropwise condensation heat transfer of steam on self-assembled monolayers, condensation experiments could also be performed at different steam velocities passing through the surface. It is anticipated that steam velocity might also affect the stability of SAMs.

In many industrial applications, steam condensation occurs in vacuum conditions. Thus, it would be very interesting to relate the changes of heat transfer coefficient over time, heat flux and steam velocity with surface properties and chemistries of SAMs under vacuum conditions.

The application of SAMs for DWC promoters, fabrication of sensors, protective layers, surface devices, and patternable materials largely depends on the thermal stability of SAMs. However, it was noted that the deterioration of alkanethiol SAMs under thermal stress has been addressed in the literature, but only at atmosphere conditions. Therefore, the thermal stability of different alkanethiol SAMs under steam condensation conditions is also relevant to the present investigation.

REFERENCE

[1] E. Schmidt, W. Schurig, and W. Sellschopp. Versuche uber die kondensation von wasserdampf in film und tropfenform. *Tech. Mech. Thermodynam.*, 1:53–63, 1930.

[2] R. Erb and E. Thelen. Dropwise Condensation. Technical report, 1965. Washington, DC.

[3] D. W. Woodruff and J. W. Westwater. Steam condensation on electroplated gold: Effect of plating thickness. *Int. J. Heat Mass Transfer*, 22:629–632, 1979.

[4] G. A. O'Neill and J. W. Westwater. Dropwise Condensation of steam on electroplated silver surfaces. *Int. J. Heat Mass Transfer*, 27:1539–1549, 1984.

[5] M. Bernett and W. Zisman. Confirmation of spontaneous spreading by water on pure gold. *J. Phys. Chem.*, 74:2309–2312, 1970.

[6] D. W. Woodruff and J. W. Westwater. Steam condensation on various gold surfaces. *ASME J. Heat Transfer*, 103:685–692, 1981.

[7] P. J. Marto, D. J. Looney, J. W. Rose, and A. S. Wanniarachchi. Evaluation of organic coating for the promotion of Dropwise Condensation of steam. *Int. J. Heat Mass Transfer*, 29(8):1109–1117, 1986.

[8] K. M. Holden, A. S. Wanniarachchi, P. J. Marto, D. H. Boone, and J. W. Rose. The use of organic coatings to promote Dropwise Condensation of

steam. *ASME J. Heat Transfer*, 109(3):768–774, 1987.

[9] X. Ma, D. Xu, and J. Lin. A study of Dropwise Condensation on the ultra-thin polymer surfaces. *Heat Transfer*, 3:359–364, 1994.

[10] X. Ma, B. Wang, D. Xu, and J. Lin. Lifetime test of Dropwise Dondensation on polymer-coated surfaces. *Heat Trans. Asian Res.*, 28(7):551–558, 1999.

[11] X. Ma, J. Chen, D. Xue, J. Lin, C. Ren, and Z. Long. Influence of processing conditions of polymer film on Dropwise Condensation heat transfer. *Int. J. Heat Mass Transfer*, 45(16):3405–3411, 2002.

[12] A. Taniguchi and Y. H. Mori. Effectiveness of composite copper/graphite fluoride platings for promoting Dropwise Condensation of steam: A preliminary study. *Int. Comm. Heat Mass Transfer*, 21(5):619–627, 1994.

[13] Q. Zhao, D. Zhang, J. Lin, and G. Wang. Dropwise Condensation on *L-B* film surface. *Chem. Eng. Proc.*, 35:473–477, 1996.

[14] D. Y. Kwok and A. W. Neumann. *Contact Angle Techniques and Measurements in Surface Characterization Methods: Principles, Techniques, and Applications.* Surfactant Science Series 87. Marcel Dekker, 1st edition, 1999.

[15] A. K. Das, H. P. Kilty, P. J. Marto, G. B. Andeen, and A. Kumar. The use of an organic Self-Assembled Monolayer coating to promote Dropwise Condensation of steam on horizontal tubes. *ASME J. Heat Transfer*, 122(2):278–286, 2000.

[16] A. K. Das, H. P. Kilty, P. J. Marto, A. Kumar, and G. B. Andeen. Dropwise Condensation of steam on horizontal corrugated tubes using an organic Self-Assembled Monolayer coating. *Enhanced Heat Transfer*, 7:109–123, 2000.

[17] J.-M. Lehn. Perspectives in supramolecular chemistry-from molecular recognition towards molecular information processing and self-organization. *Angew. Chem. Int. Ed. Engl.*, 29:1304–1309, 1990.

[18] G. M. Whitesides, J. P. Mathias, and C. T. Seto. Molecular Self-Assembly and nanochemistry: A chemical strategy for the synthesis of nanostructures. *Science*, 254:1312–1319, 1991.

[19] J.-M. Lehn. Supramolecular chemistry-scope and perspectives molecules, supramolecules, and molecular devices (Nobel lecture). *Angew. chem. Int. Ed. Engl.*, 27:89–112, 1988.

[20] C. A. Mirkin, R. L. Letsinger, R. C. Mucic, and J. J. Storhoff. A DNA-based method for rationally assembling nanoparticles into macroscopic materials. *Nature*, 382:607–609, 1996.

[21] A. P. Alivisatos, K. P. Johnsson, X. Peng, T. E. Wilson, C. J. Loweth, M. P. Bruchez Jr, and P. G. Schultz. Organization of 'Nanocrystal Molecules' using DNA. *Nature*, 382:609–611, 1996.

[22] A. S. Dimitrov and K. Nagayama. Continuous convective assembling of fine particles into two-dimensional arrays on solid surfaces. *Langmuir*, 12:1303–1311, 1996.

[23] N. Bowden, A. Terfort, J. Carbeck, and G. M. Whitesides. Self-Assembly of mesoscale objects into ordered two-dimensional arrays. *Science*, 276:233–235, 1997.

[24] G. M. Whitesides and P. E. Laibinis. Wet chemical approaches to the characterization of organic surfaces: Self-Assembled Monolayers, wetting, and the physical-organic chemistry of the solid-liquid interface. *Langmuir*, 6:87–96, 1990.

[25] J. Xu and H.-L. Li. The chemistry of Self-Assembled long-chain Alkanethiol monolayers on gold. *J. Coll Interf. Sci.*, 176:138–149, 1995.

[26] H. Sellers, A. Ulman, Y. Shnidman, and J. E. Eilers. Structure and binding of Alkanethiolates on gold and silver surface: Implications for Self-Assembled Monolayers. *J. Am. Chem. Soc*, 115:9389–9401, 1993.

[27] Y. Xia and G. Whitesides. Soft lithography. *Angew. Chem. Int. Ed.*, 37:550–575, 1998.

[28] R. G. Nuzzo and D. L. Allara. Adsorption of bifunctional organic disulfides on gold surfaces. *J. Am. Chem. Soc.*, 105:4481–4483, 1983.

[29] M. M. Walczak, C. Chung, S. M. Stole, C. A. Widrig, and M. D. Porter. Structure and interfacial properties of spontaneously adsorbed *n*-Alkanethiolate monolayers on evaporated silver surfaces. *J. Am. Chem. Soc.*, 113:2370–2378, 1991.

[30] P. E. Laibinis and G. M. Whitesides. Self-Assembled Monlayers of *n*-Alkanethiolates on copper are barrier films that protect the metal against oxidation by air. *J. Am. Chem. Soc.*, 114:9022–9028, 1992.

[31] P. E. Laibinis and G. M. Whitesides. ω-Terminated Alkanethiolate monolayers on surfaces of copper, silver, and gold have similar wettabilities. *J. Am. Chem. Soc.*, 114:9022–9028, 1992.

[32] N. Muskal, I. Turyan, A. Shurky, and D. Mandler. Chiral Self-Assembled Monolayers. *J. Am. Chem. Soc.*, 117:1147–1148, 1995.

[33] M. Stratmann. *Adv. Mater.*, 29:191, 1990.

[34] Y. Li, J. Huang, J. R. T. McIver, and J. C. Hemminger. Characterization of thiol Self-Assembled films by laser desorption Fourier Transform Mass Spectrometry. *J. Am. Chem. Soc.*, 114:2428–2432, 1992.

[35] C. D. Bain, E. B. Troughton, Y. Tao, J. Evall, G. M. Whiteside, and R. G. Nuzzo. Formation of monolayer film by the spontaneous assembly of organic thiols from solution onto gold. *J. Am. Chem. Soc.*, 111:321–335, 1989.

[36] J. Yang, J. Han, K. Isaacson, and D. Y. Kwok. Effects of surface defects, polycrystallinity, and nanostructure of self-assembled monolayers for octadecanethiol adsorbed onto au on wetting and its surface energetic interpretation. *Langmuir*, 19:9231–9238, 2003.

[37] Chao Yang. Corrosion protection of copper by self-assembled monolayers. Master's thesis, University of Alberta, 2002.

[38] M. R. Vogt, F. A. Möller, C. M. Schilz, O. M. Magnussen, and R. J. Behm. Adsorbate-induced step faceting of Cu(100) electrodes in HCI. *Surf. Sci*, 367:L33–L41, 1996.

[39] M. R. Vogt, A. Lachenwitzer, O. M. Magnussen, and R. J. Behm. In-situ STM study of the initial stages of corrosion of Cu(100) electrodes in sulfuric and hydrochloric acid solution. *Surf. Sci*, 399:49–69, 1998.

[40] J. Scherer, M. R. Vogt, O. M. Magnussen, and R. J. Behm. Corrosion of Alkanethiol-covered Cu(100) surface in hydrochloric acid solution studied by in-situ scanning tunneling microscopy. *Langmuir*, 13:7045–7051, 1997.

[41] M. Itoh, H. Nishihara, and K. Aramaki. The protection ability of 11-Mercapto-1-Undecanol Self-Assembled Monolayer modified with Alkyltrichlorosilanes against corrosion copper. *J. Electrochem. Soc.*, 142:1839–1846, 1995.

[42] Y. Feng, W. K. Teo, K. S. Siow, Z. Gao, K. L. Tan, and A. K. Hsieh. Corrrosion protection of copper by a Self-Assembled Monolayer of Alkanethiol. *J. Electrochem. Soc.*, 144:55–63, 1997.

[43] R. G. Nuzzo, F. A. Fusco, and D. L. Allara. Spontaneously organized molecular assemblies. 3. preparation and properties of solution adsorbed monolayers of organic disulfides on gold surfaces. *J. Am. Chem. Soc.*, 109:2358–2368, 1987.

[44] D. M. Jaffey and R. J. Madix. Reactivity of sulfur-containing molecules on nobel metal surfaces. 2. *tert*-Butyl Thioalcohol on Au(110). *J. Am. Chem. Soc.*, 116:3012–3019, 1994.

[45] P. Fenter and P. Eisenberger. Chain-length dependence of the structures and phases of $CH_3(CH_2)_{n-1}SH$ Self-Assembled on Au(111). *Phys. Rev. Lett.*, 70:2447–2450, 1993.

[46] F. Seker, K. Meeker, T. F. Kuech, and A. B. Ellis. Surface chemistry of prototypical bulk II-VI and III-V semiconductors and implications for chemical sensing. *Chem. Rev.*, 100:2505–2536, 2000.

[47] E. Delamarche, B. Michel, H. Kang, and C. Gerber. Thermal stability of Self-Assembled Monolayers. *Langmuir*, 10:4103–4108, 1994.

[48] A. Kumar, H. A. Biebuyck, and G. M. Whitesides. Patterning Self-Assembled Monolayers: Applications in materials science. *Langmuir*, 10:1498–1511, 1994.

[49] J. B. Schlenoff, M. Li, and H. Ly. Stability and self-exchange in Alkanethiol monolayers. *J. Am. Chem. Soc.*, 117:12528–12536, 1995.

[50] R. E. Johnson Jr. and D. H. Dettre. Wettability and contact angles. In E. Matijévic, editor, *Surface and Colloid Science*, pages 85–153. Wiley, New York, 1969.

[51] A. M. Schwartz, C. A. Rader, and E. Huey. Contact angle wettability and adhesion: Resistance to flow in capillary system of positive contact angle. In

R. F. Gould, editor, *Advances in Chemistry Series*, volume 43, pages 250–267. American Chemical Society, Washington, D. C., 1964.

[52] C. G. L. Furmidege. The sliding of liquid drops on solid surfaces and a theory for spray retention. *J. Colloid Sci.*, 17:309, 1962.

[53] A. H. Abdelmessih, A. W. Neumann, and S. W. Yang. The effect of surface characteristics on Dropwise Condensation. *Let. Heat Mass Transfer*, 2:337, 1975.

[54] A. W. Neumann, A. H. Abdelmessih, and A. Hameed. The role of contact angles and contact angle hysteresis in Dropwise Ccondensation heat transfer. *Int. J. Heat Mass Transfer*, 21:947, 1978.

[55] A. W. Neumann. Contact angles and their temperature dependence: Thermodynamic status, measurement, interpretation and application. *Adv. colloid Interface Sci.*, 4:105, 1974.

[56] C. Graham. *The limiting Heat Transfer Mechanism of Dropwise Condensation of Steam.* PhD thesis, Massachusetts Institute of Technology, 1969.

[57] C. Graham and P. Griffith. Drop size distributions and heat transfer in Dropwise Condensation. *Int. J. Heat Mass Transfer*, 16:337, 1973.

[58] I. Tanasawa and J. Ochiai. Experimental study on Dropwise Condensation. *Bull. JSME*, 16:1184, 1973.

[59] I. Tanasawa. Dropwise Condensation: the way to practical applications. In *The Sixth International Heat Transfer Conference*, pages 393–405, Toronto, Canada, 1978.

[60] D. M. Mattox. *Handbook of Physical Vapor Deposition (PVD) Processing.* Noyes Publications, 1998.

[61] F. M. White. *Fluid Mechanics.* McGraw-Hill, Inc., 2 edition, 1986.

[62] D. W. Tanner, D. Pope, C. J. Potter, and D. West. Heat transfer in Dropwise Condensation-part I: The effect of heat flux, steam velocity and non-condensable gas concentration. *Int. J. Heat Mass Transfer*, 8:419–426, 1965.

[63] F. S. Tse and I. E. Morse. *Measurement and Instrumentation in Engineering: Principles and Basic Laboratory Experiments.* M. Dekker, Inc., New York, 1989.

[64] F. P. Incropera and D. P. DeWitt. *Introduction to Heat Transfer - 3rd Ed.* John Wiley & Sons, 1996.

[65] H. Ron, S. Matlis, and I. Rubinstein. Self-Assembled Monolayers on oxidized metals: 2. gold surface oxidative pretreatment, monolayer properties, and depression formation. *Langmuir*, 14:1116–1121, 1998.

[66] P. E. Laibinis, G. M. Whitesides, D. L. Allara, Y. T. Tao, A. N. Parikh, and R. G. Nuzzo. *J. Am. Chem. Soc.*, 113:7152, 1991.

[67] G. K. Jennings and P. E. Laibinis. Self-Assembled n-Alkanethiolates monolayers on underpotentially deposited adlayers of silver and copper on gold. *J. Am. Chem. Soc.*, 119:5208–5214, 1997.

[68] R. G. Nuzzo, L. H. Dubois, and D. L. Allara. Fundamental studies of microscopic wetting on organic surfaces. *J. Am. Chem. Soc.*, 112:558–569, 1990.

[69] G. K. Jennings, J. C. Munro, T. Yong, and P. E. Laibinis. Effect of chain length on the protection of copper by n-Alkanethiols. *Langmuir*, 14:6130–6139, 1998.

[70] P. Griffith. *Handbook of Heat Transfer.* McGraw-Hill, Toronto, 1973.

[71] J. W. Rose. Condensation heat transfer. *Heat and Mass Transfer*, 35:479–485, 1999.

[72] I. Tanasawa. Advances in condensation heat transfer. *Advances in Heat Transfer*, 21:55–139, 1991.